

GRI-03/0065 vol. 5

**Seal Control of Hydrocarbon Migration and its Physical and
Chemical Consequences**

**VOLUME V: A MODELING ANALYSIS OF THE HYDROCARBON CHEMISTRY AND GAS
WASHING, HYDROCARBON FLUXES, AND RESERVOIR FILLING**

FINAL TECHNICAL REPORT
(6/19/1997-12/31/2001)

Prepared by:
L. M. Cathles and S. L. Losh

Cornell University
Department of Earth & Atmospheric Sciences
Snee Hall
Ithaca, NY 14853

OSP #32006

Prepared for:

GAS RESEARCH INSTITUTE
5097-260-3787

December 2002

REPORT DOCUMENTATION PAGE

Form Approved
OMB No. 0704-0188

Public reporting burden for this collection of information is estimated to average 1 hour per response, including the time for reviewing instructions, searching data sources, gathering and maintaining the data needed, and completing and reviewing the collection of information. Send comments regarding this burden estimate or any other aspect of this collection of information, including suggestions for reducing this burden to Washington Headquarters Service, Directorate for Information Operations and Reports, 1215 Jefferson Davis Highway, Suite 1204, Arlington, VA 22202-4302, and to the Office of Management and Budget, Paperwork Reduction Project (0704-0188) Washington, DC 20503.

PLEASE DO NOT RETURN YOUR FORM TO THE ABOVE ADDRESS.

1. REPORT DATE (DD-MM-YYYY)			2. REPORT DATE		3. DATES COVERED (From - To)	
4. TITLE AND SUBTITLE				5a. CONTRACT NUMBER		
				5b. GRANT NUMBER		
				5c. PROGRAM ELEMENT NUMBER		
6. AUTHOR(S)				5d. PROJECT NUMBER		
				5e. TASK NUMBER		
				5f. WORK UNIT NUMBER		
7. PERFORMING ORGANIZATION NAME(S) AND ADDRESS(ES)					8. PERFORMING ORGANIZATION REPORT NUMBER	
9. SPONSORING/MONITORING AGENCY NAME(S) AND ADDRESS(ES)					10. SPONSOR/MONITOR'S ACRONYM(S)	
					11. SPONSORING/MONITORING AGENCY REPORT NUMBER GRI-03/0065 vol. 5	
12. DISTRIBUTION AVAILABILITY STATEMENT						
13. SUPPLEMENTARY NOTES						
14. ABSTRACT						
15. SUBJECT TERMS						
16. SECURITY CLASSIFICATION OF:			17. LIMITATION OF ABSTRACT	18. NUMBER OF PAGES	19a. NAME OF RESPONSIBLE PERSON	
a. REPORT	b. ABSTRACT	c. THIS PAGE			19b. TELEPHONE NUMBER (Include area code)	

GRI Disclaimer

LEGAL NOTICE

This report was prepared by Cornell University as an account of contracted work sponsored by the Gas Research Institute (GRI). Neither Cornell University, GRI, members of these companies, nor any person acting on their behalf:

- a. Makes any warranty or representation, expressed or implied, with respect to the accuracy, completeness, or usefulness of the information contained in this report, or that the use of any apparatus, methods, or process disclosed in this report may not infringe upon privately owned rights; or
- b. Assumes any liability with respect to the use of, or for damages resulting from the use of, any information, apparatus, method, or process disclosed in this report.

Table of Contents

Report Documentation Page (SF 298)	2
GRI Disclaimer	3
Table of Contents	4
Research Summary	6
Technical Section	10
A. Summary.....	10
B. Introduction.....	11
C. Physical Modeling Methods	12
1. Plate Models.....	12
2. Parameter Models	16
a. Thermal Conductivity.....	16
b. Porosity	17
c. Permeability	17
d. Radiogenic Heat Production	18
3. Thermal Models.....	18
4. Chemical Modeling Methods.....	19
a. Hydrocarbons Maturation Models	19
b. Hydrocarbons and Brine Migration Models	21
D. Modeling Results	22
1. A 1050 km Long Section Across the Entire Offshore Louisiana Basin.....	22
a. Physical Evolution of the 1050 km Section.....	22
b. Thermal Evolution	24
c. Discussion.....	28
2. A 200 km 2D N-S Line Across the GRI Corridor	28
a. Transfer of Louisiana Section Boundary Conditions.....	28
b. Geochemical Constraints: Gas Washing, Oleanane and Sulfur.....	31
c. Hydrocarbon Generation Potential	34
d. Hydrocarbon Maturation, Migration, and Venting.....	35
e. Computed Hydrocarbon Chemistry	38
f. Reservoir Filling and Washing at the 4 Corridor Sites.....	44
1) Tiger Shoals	44
2) South Marsh Island 9	55
3) Eugene Island Block 330	56
4) Jolliet.....	56
5) Corridor Characteristics	56

E. Summary, Discussion, and Future Work	57
1. Summary	57
2. Discussion	59
3. Future Work	60
Acknowledgements	61
References Cited.....	62

Research Summary

TITLE: A Modeling Analysis of the Hydrocarbon Chemistry and Gas Washing, Hydrocarbon Fluxes, and Reservoir Filling

CONTRACTOR: Cornell University

PRINCIPAL INVESTIGATOR: Lawrence M. Cathles III

REPORT PERIOD: January 1, 1997 to December 31, 2001

OBJECTIVES: The objectives of this report are to:

- (1) describe basin and hydrocarbon models we have constructed,
- (2) describe how these models have been used to determine the amounts and rates of hydrocarbon maturation, past and present hydrocarbon fluxes, and the amounts of gas available for gas washing of oil in the offshore Louisiana Gulf of Mexico Corridor, and
- (3) draw conclusions regarding the operation of the hydrocarbon system from the pattern of gas washing in the GRI Corridor.

TECHNICAL PERSPECTIVE: The interior of the northern offshore Gulf of Mexico Basin is divided into a complex system of variously over-pressured compartments. It is an area of active hydrocarbon generation and one of the world's most active areas of hydrocarbon exploration. There is no present consensus on how hydrocarbons migrate through these pressure compartments, the nature of the impermeable seals that separate the compartments, and how the flow of gas and brine affect hydrocarbon chemistry and inorganically alter sediments. However, a newly-documented, coherent pattern of gas washing and chemical change [volume IV] provide powerful constraints on the style of hydrocarbon migration in this part of the Gulf of Mexico Basin. These constraints are made clear by the modeling reported here.

RESULTS: We show that rifting basin models with no free parameters reproduce both the unusually low surface heat flow (~half normal) and present temperature gradients in the GRI Corridor. The models take into account radiogenic heat production in the basin sediments and in the continental crust below. The low heat flow is due to rapid deposition of cold sediments. The analysis confirms

the low values of shale thermal conductivity used in some, but not all, published models.

Hydrocarbon maturation calculated for the model thermal history shows that 184 billion tonnes of mobile hydrocarbons have been generated in the GRI Corridor over the last 25 Ma, of which ~146 Bt have been expelled from the source strata, and ~131 Bt vented into the ocean. The 1.37 Bt of discovered recoverable hydrocarbons in the Corridor are <1% of those expelled from source strata.

The remarkable pattern of gas washing observed in the Corridor (a smooth variation from 90 wt% n-alkane mass removed in the north and 0% removed in the south) is naturally accounted for by hydrocarbon migration models provided there is very little (<0.05 vol %) retention of hydrocarbons in the migration pathways. If this is the case, late gas can interact at high enough gas-oil ratio with oils migrated earlier to wash the hydrocarbons as observed. The washing must occur near present reservoir depths (washing break number constraints discussed in Volume IV). The observed gas-oil ratios cannot be attained if too large a volume of hydrocarbon occupies the source-to-reservoir migration pathways. The retention of hydrocarbons in the migration pathways must therefore be low (~0.05 %). The retention must also be low for Eocene oils to displace earlier-generated Jurassic oils in the northern part of the Corridor, as observed. Lack of biodegradation of the reservoired hydrocarbons and other geological constraints require that the reservoirs were filled very recently. This can be done from current hydrocarbon generation provided hydrocarbons are drawn to reservoirs from distances similar to that of salt-withdrawal minibasins in the Corridor (draw radius of 10 to 20 km).

The picture that emerges from the modeling analysis is one in which hydrocarbons are generated and vented into the ocean with very little out-of-source retention. The GRI Corridor is a massively leaky flow-through hydrocarbon system in which >100 times more hydrocarbons are expelled into the ocean than are retained in discovered commercial reservoirs. The chemical pattern of gas washing is compatible with this scenario and only with this scenario.

**TECHNICAL
APPROACH:**

Conclusions are drawn by modeling hydrocarbon generation, migration, and gas washing. The thermal history of the Corridor is calculated from basal heat flow specified by a lithosphere-scale rift model. The rift extension is estimated from isostasy, present-day

water depth and sediment thickness. The plate model computes the thermal effects of stretching a 150 km thick crust-lithosphere plate and then depositing sediments at the geologically observed rates, taking into account radiogenic heat production in the crust and basin sediments. The thermal history of Corridor sediment is then computed using basal heat flow specified by this plate model. Temperature at the sea floor is specified by water depth relative to the thermocline in the present Gulf.

The temperature history is then used to mature Jurassic and Eocene source rocks in the Corridor. The model hydrocarbons are migrated assuming that expulsion from source strata requires a 20 vol% hydrocarbon saturation of the pore space, and assuming that migration thereafter requires a <0.05 vol% pore space saturation. Migration gas-oil mass ratios decrease from north to south across the Corridor. This variation provides a natural explanation for the variation in the intensity of gas washing that is observed across the Corridor (90 wt% removal of n-alkanes in the north, ~0% in the south). The draw area required to fill reservoirs in 4 Corridor study areas (Tiger Shoals, Sount Marsh Island 9, South Eugene Island Block 330 area, and Jolliet) in geologically- or biologically- indicated time periods is computed by dividing the reservoired hydrocarbon mass by the product of this filling time and the average model hydrocarbon flux over this time.

**PROJECT
IMPLICATIONS:**

The model analysis of gas washing indicates that hydrocarbons have been very recently introduced into the Corridor reservoirs and that the introduction has been increasingly recent to the south. Once established, one site on the margins of a salt-withdrawal minibasin appears to become the principal site of hydrocarbon discharge, and this site seems then to persist and vent most of the hydrocarbons generated beneath the minibasin. Exploration near these persistent vents, which are topographic highs in the top of overpressure, should provide a higher probability of encountering reservoirs that are filled with hydrocarbons. The chemistry of the hydrocarbons has been dramatically affected by gas washing in the north of the Corridor. Gas washing removes light-end alkanes and could also cause other economically important chemical changes such as asphaltene precipitation.

**PROJECT
MANAGERS:**

Richard Parker and Robert Siegfried

Technical Section

A. Summary

Oleanane and sulfur contents of 138 un-biodegraded oils in a 125×200 km area of the offshore Louisiana Gulf of Mexico Basin (which we call the GRI Corridor) suggests that oils there are sourced from Type II Jurassic and Type III Eocene kerogens (Volume II of this series). Eocene-sourced oils dominate the northern part of the study area; only Jurassic-sourced oils are present in the south. The oils in the north are highly altered. Up to 90 wt% of their n-alkanes have been removed by washing with gas (Volume IV this series).

We use a two-source basin model to analyze this data. The history of sediment deposition and salt diapirism is reconstructed over the last 144 Myrs for a section published by McBride (1998) that lies ~ 50 km east of the GRI Corridor. With radiogenic heat generation and the effects of rifting and rapid sedimentation taken into account, the model predicts the heat flow and temperature gradients observed. We assume a Jurassic Type II source 100 m thick layer extending across the full 200 km N-S section at the top of the Louann salt. This source bed contains 5 wt% TOC and has an HI of 628 mg/g. The model Eocene Type III source is 30 m thick, extends only under the northern half of the section, has 4 wt% TOC, and an HI of 205 mg/g. A 20 vol% hydrocarbon saturation is required for hydrocarbons to be expelled from the model source strata. The hydrocarbon saturation required for migration is treated as a parametric variable.

The model analysis shows that the pattern of oil chemistry and alteration can be reproduced in all aspects if (and probably only if) the migration hydrocarbon saturation is $<0.05\%$. A migration saturation $<0.5\%$ is required for hydrocarbons to vent to the surface; an order of magnitude lower migration saturation is required for Eocene oils to dominate the oil chemistry in the northern part of the study area, and for these oils to be washed by Jurassic-sourced gas to the extent observed. The analysis suggests a flow-through system in which very little hydrocarbon is retained in the migration pathways and almost all the mobile hydrocarbons generated are vented into the ocean. In the 125×200 km area, 131 Bt (billion tonnes) or $\sim 1000 \times 10^9$ bboe of model hydrocarbons have vented into the ocean, 37 Bt are retained in the source strata, and 15 Bt are retained in the migration pathways. About 1.4 Bt of hydrocarbons have been discovered in producible reservoirs in the Corridor. The lack of biodegradation and other geological constraints indicates that the hydrocarbons in producing areas have accumulated recently. The hydrocarbons can accumulate in the required times if drawn from areas similar in size to the salt-withdrawal minibasins that control the recent sedimentation pattern. The venting rate predicted at Jolliet/Bush Hill for this draw is compatible with the rate of gas venting independently estimated from the Bush Hill hydrate accumulation that is structurally connected to the Jolliet reservoirs.

B. Introduction

This report documents results from numerical models of the maturation and migration of hydrocarbons in the GRI Corridor, a 125×250 km area in the offshore Louisiana Gulf of Mexico. The models are used to investigate the interaction of late-generated gas with earlier-generated oil. We seek to understand the dramatic pattern of gas washing observed in this area. This report is one in a series of reports that describe our efforts to understand physical and chemical processes in the GRI Corridor. The report series is “Seal Control of Hydrocarbon Migration and its Physical and Chemical Consequences.” The six (6) volumes that comprise this report are:

- Volume I: Executive Summary
- Volume II: Geology, Geophysics, Geochemistry and GoCAD Database
- Volume III: Organic Geochemistry
- Volume IV: Gas Washing of Oil and Its Implications
- Volume V: A Modeling Analysis of the Hydrocarbon Chemistry and Gas Washing, Hydrocarbon Fluxes, and Reservoir Filling
- Volume VI: A Theoretical Analysis of the Inorganic Alteration by the Flow of Brines Through Basin Seals

Now published reports from a preceding GRI project describe our concepts of capillary sealing (Cathles, 2001), laboratory investigations of capillary sealing (Shosa and Cathles, 2001), methods for interpreting the history of fluid overpressuring from porosity profiles (Revil and Cathles, 2001), geochemical models of phase fractionation (Meulbroek, 1997; Meulbroek, 1998), and implications of capillary sealing for oil production (Erendi and Cathles, 2001).

Our purpose in this report is to describe how we have used models to extract information from geological and geochemical observations in the GRI Louisiana Corridor. Models are used to determine the amounts and rates of hydrocarbon generation in the Corridor, the changes in the gas-oil ratio that occurred over time, and the timing of reservoir filling. The models provide a basis for evaluating gas washing, capillary seal development, and inorganic alteration.

Modeling of the GRI Corridor is carried out at telescoping scales. On the largest scale, we model a 1050 km long 2D section through Louisiana that stretches from the Arkansas border (~450 km onshore) to the Sigsbee Knolls (~600 km offshore). This defines heat flow over the last 150 Myrs, tests models of thermal conductivity, and allows the temperature history of the Corridor to be defined with considerable precision and confidence. The temperature history is then used, together with a maturation model and estimates of the distribution of source rocks, to predict the history of hydrocarbon generation and mixing across the 200 km N-S GRI Corridor.

Discussion is divided into two sections. The first (Physical Modeling Methods) section discusses the construction of the models and the many parameters they require. For example, heat flow must be defined over the basin’s history because it determines basin temperature and hydrocarbon maturation. The thermal conductivity of the sediments must therefore be known as a function of lithology, porosity, temperature, and perhaps

hydrocarbon saturation because it controls basin temperature. For the same reason, radiogenic heat production must be accounted for both within the basin and in the continental crust that underlies the basin. To simulate hydrocarbon generation the cracking of kerogen to oil and then gas and the breakdown of oil to gas must be described by kinetic maturation models. The second (Modeling Results) section discusses the application of the models to the GRI Corridor and draws conclusions. The first section can be skipped, skimmed, or consulted only as needed by readers most interested in the results.

C. Physical Modeling Methods

Four kinds of models are needed :

1. A *Plate Model* is needed to calculate the heat flow into the base of the sedimentary section from the mantle. This model must take into account the thickening of the lithosphere after rifting, radiogenic heat generation in the crust, and the cooling effects of sedimentation.
2. *Parameter Models* are needed to describe compaction of basin sediments as they are buried and to calculate material properties as a function of compaction (porosity), lithology, and temperature.
3. *Thermal Models* are needed to calculate the temperature in the accumulating sediments.
4. *Hydrocarbon Models* are needed to calculate the cracking of buried organic carbon into oil and gas, the cracking of oil to gas, the volume change associated with these reactions, and the movements of hydrocarbon and aqueous fluids in response to compaction and the positive-volume maturation reactions.

1. Plate Models

Heat flow into the base of sedimentary basins must be defined before the thermal history of the basin sediments can be calculated. This heat flow is from two sources: cooling of the mantle (thickening of the lithosphere) and radioactive decay in the crust below the basin sediments. Deposition of cold sediments can have a dramatic cooling effect, and greatly depress the heat flow to the base of a sedimentary section, but models that consider the entire lithosphere are necessary to capture this cooling effect (Hutchison, 1985). Our approach is to infer the thinning of the crust and lithosphere from the change in water depth and the sediment accumulation that has occurred since rifting, following the methods of McKenzie (1978), Royden, Sclater et al. (1980) and Watts (1981). We then calculate the heat flow to the base of the accumulating sedimentary section using a one-dimensional, finite-element plate model similar to the finite-difference model described in Hutchison (1985).

Specifically, the beta factor, β , characterizing the thinning of the crust and lithosphere by pure shear is related to the change in water depth, $\Delta W_D(t_r)$ and the sediment accumulation $\Delta S_S(t_r)$ in the time that has elapsed since rifting, t_r :

$$1 - \frac{1}{\beta} = \frac{\frac{\Delta S_S(t_r)}{m} + \Delta W_D(t_r)}{S_{IW} + S_{TW\infty} \left(1 - \exp\left(-\frac{t_r}{\tau}\right)\right)} \quad (1)$$

The parameters in equation (1) are defined in Table 1.

The beta factor calculated from equation (1) allows us to define a lithospheric plate cooling model. There are four layers in the plate model: the basin, the crust, the lithosphere below the crust, and the asthenosphere. The asthenosphere is assumed to have constant temperature, T_{asth} , of 1350°C (see Table 1). The lithosphere (solidified asthenosphere) is assumed to have no significant radioactive heat generation, but heat generation is included in the crust.

The radiogenic heat generation at the top of the crust before rifting is A_{crust} . Radiogenic heat generation decays with depth in the crust such that $A(z) = A_{crust} \exp(-z/\delta_{crust})$, where z is the depth below the top of the crust (positive downward), and A_{crust} is as defined in Table 1.

When rifting takes place the crust and lithosphere are reduced in thickness by β . The exponential decay of radiogenicity in the crust is adjusted so that the total heat generation in the thinned crust is reduced by β . The heat generation rate at the top of the crust is kept unchanged. The crust, lithosphere and asthenosphere have the same thermal properties except that the crust includes radiogenic heat production. Initial temperature profiles are established in the rifted crust and lithosphere as described below. Sediments are then added to the crust, and the warming of these sediments and cooling of the crust and lithosphere is calculated using finite element techniques. Compaction and heat production are accounted for in the basin sediments. The numerical methods are elaborated below but are very similar to those used by Hutchison (1985), except that we use a coordinate system attached to the solid matrix.

Table 1. Definition of parameters in equation (1), the plate model, and in thermal modeling. Parameter values are from (Royden, Sclater et al., 1980; Sass, Brott et al., 1981; Watts, 1981; Hutchison, 1985) as discussed in text.

Variable	Definition	Value or Expression
β	Crustal thinning: ratio of the pre-rifting thickness of crust or lithosphere to the post-rifting thickness	Calculate from equation (1)
$\Delta S_s(t_r)$	Change in thickness of sedimentary section since rifting at location where β is calculated	Observed value
$\Delta W_D(t_r)$	Change in water depth since rifting at location where β is calculated	Observed value
t_r	Time since rifting	158 Ma
a	Pre-rifting thickness of the crust plus lithosphere	150 km
h_c	Pre-rifting thickness of the crust	28 km
ρ_w	Density of water, equivalent to seawater	1.03 g/cc
ρ_{mo}	Density of the mantle at 0°C	3.33
ρ_{co}	Density of the crust at 0°C	2.8
α	Coefficient of thermal expansion	3.3×10^{-5}
T_{asth}	Temperature at the top of the asthenosphere	1350°C
ρ_m	Density of the top to the asthenosphere	$\rho_{mo}(1 - \alpha T_{asth})$
ρ_s	Average sediment density	2.2 g/cc
$\bar{\rho}_c$	Average density of crust	$\rho_{co} \left(1 - \frac{\alpha T_{asth} h_c}{2a} \right)$
$\bar{\rho}_l$	Average density of lithosphere	$\rho_{co} \left(1 - \frac{\alpha T_{asth}}{2} \left(1 + \frac{h_c}{a} \right) \right)$
S_{IW}	Initial water-loaded subsidence divided by $1 - 1/\beta$	$\frac{a(\rho_m - \bar{\rho}_l) + h_c(\bar{\rho}_l - \bar{\rho}_c)}{\rho_m - \rho_w}$
$S_{TW\infty}$	Ultimate thermal subsidence divided by $1 - 1/\beta$	$\sim \frac{a\rho_m\alpha T_{asth}}{2(\rho_m - \rho_w)}$
τ	Thermal decay time of the lithosphere	62 Ma
A_{crust}	Heat generation at top of crust	7.64×10^{-13} cal/cm ³ -sec
δ_{crust}	Skin depth of radiogenicity in crust	7.5 km
K_{lith}	Thermal conductivity of crust and lithosphere	7.5×10^{-3} cal/cm-sec-C
$\bar{\rho}_l c$	Heat capacity of crust and lithosphere	0.89 cal/cm ³
R_{flex}	Flexural rigidity of lithosphere	10^{23} N-m
T_{water}	Temperature of water above the thermocline	20°C
T_{amb}	Ambient air temperature (yearly average)	20°C
$T_{deepwater}$	Deep water temperature	4.5°C
D_{tmclt}	Depth to the top of the thermocline	80 m
D_{tmclb}	Depth to the base of the thermocline	570 m
m	Magnification of water-loaded subsidence by sediment load	$\frac{\rho_m - \rho_w}{\rho_m - \rho_s}$

The cooling calculations are one dimensional. The finite-element node spacing increases with depth below the top of the crust such that the spacing between each successive node increases by a factor of 1.5. The total number of nodes spanning the crust and mantle is 20. The lithosphere nodes span the full pre-rift thickness of the lithosphere. When rifting occurs, the lithosphere is “thinned” in the sense that the temperature in the lithosphere below a depth of a/β , where a is the pre-rift thickness of the lithosphere, is set at T_{asth} . After rifting, additional basin nodes are added as sedimentary layers are deposited.

Changes in the thermal conductivity of the basin sediments that occur as they compact and are warmed are taken into account in the model, as is radiogenic heat generation in the basin sediments. Compaction is calculated assuming hydrostatic pore pressures as described in the next section. Standard finite element techniques (Baker and Pepper, 1991) are used in the calculations. Two iterations are taken at each timestep to converge the temperature-dependent thermal conductivity in the basin sediments. The calculations have been verified against the conductive cooling of and initially isothermal halfspace (Carslaw and Jaeger, 1959), and against the prior models of Hutchison (1985). We also have verified that increasing the number of nodes and reducing the size of the timesteps taken do not change the computational results.

Plate model simulations start with the deposition of the first post-rifting sedimentary strata. The initial temperature profile in the basin consists four linear segments:

- from T_{surf} at the surface to T_B at the base of the sedimentary basin (top of the crust),
- from T_B at the top of the crust to T_C the base of the crust as thinned by rifting
- from T_C the base of the crust to T_{asth} at the top of the asthenosphere, and
- from T_{asth} at the top of the asthenosphere to T_{asth} at a depth equal to the initial pre-rift thickness of the lithosphere.

T_B and T_C are solved by iteratively taking into account radioactive heat generation in the crust (but not in basin sediments which have yet to be deposited).

As indicated in Table 1 we assume that the pre-rifting lithosphere thickness, a , in the Gulf of Mexico area was 150 km (Pollack and Chapman, 1977). We take the pre-rift continental crust, h_c , to be 28 km thick. From Pollack and Chapman (1977) and Sass, Brott et al. (1981), we take the surface heat generation of the pre-rift crust to be $A_{\text{crust}} = 3.2 \text{ mW/m}^3$ and the depth characterizing the exponential decay of the surface heat generation to be $\delta_{\text{crust}} = 7.5 \text{ km}$.

The plate model predicts the heat flow to the base of the sedimentary section as a function of β , the radiogenic heat production in the basin and crust, and sedimentation rate. The plate model is used to determine the proper basal heat flow boundary conditions for the basin sediment model.

2. Parameter Models

a. Thermal Conductivity

The thermal conductivity model we use is a fabric model that mixes harmonic and arithmetic averages of temperature-dependent, thermal conductivities for end-member lithologies which follows methods described in Luo, Wood et al. (1994). We adopt Platte River values for the 25°C grain (0% porosity) conductivities of the lithologic mixtures as shown in Table 2.

The thermal conductivities of the end members in Table 2 are mostly those expected. For example, according to Blatt (1992), a typical sand contains 20% feldspar, 15% mixed layer clays, and 65% quartz. Using thermal conductivities for these minerals from Horai (1971) and the fabric theory of Luo, Wood et al. (1994), we expect a 0% porosity thermal conductivity of 4.39 mW/m-K for sand, which is very close to the Platte River value in Table 2. The thermal conductivity of shale in Table 2 is much lower than expected based on such a calculation, however, which would give a value of ~ 3.05 not 1.5 mW/m-K. This major discrepancy, which alone would decrease the temperature gradient in shale-dominated deltaic basins like the Gulf of Mexico Basin by a factor of ~ 2 , requires discussion.

Table 2. Thermal conductivities of mixtures of mineral grains for various lithologies at 25°C. Matrix conductivities are those used by Platte River in their modeling. The end member grain densities, ρ_G , the uncompacted (surface) porosities, ϕ_0 , the rigidities, σ_c , and the heat generation per kg sediment, A_T are also listed.

	K[mW/m-K]	ρ_G[g/cm³]	ϕ_0	σ_c[bars]	A_T[nW/kg]
sand	4.4	2.76	0.39	1745	0.63
shale	1.5	2.76	0.35	1629	0.73
carbonate sand	2.9	2.72	0.47	814	0.15
carbonate mud	4.8	2.72	0.43	786	0.15
salt	5.4	2.16	0	10 ⁸	0

The explanation of the low values of shale thermal conductivity rests in the fact that shale thermal conductivity is often strongly anisotropic, with the thermal conductivity perpendicular to bedding having values 2.5 times lower than the thermal conductivity parallel to bedding. The values perpendicular to bedding commonly have values ~ 1 mW/m-K (Blackwell and Steele, 1989; Deming, 1994). The case has been made most strongly by Blackwell and Steele (1989) who state that “published estimates of the [vertical] thermal conductivity of shale appear to be in error by 50 to 100%”. They show that shale thermal conductivities must be between 1.1 and 1.3 mW/m-K for heat flows inferred from temperature gradients in shales to be compatible with those in sands in the same wells. Thermal conductivity measurements on shale cuttings (typically ~ 2 mW/m-K) homogenize the thermal conductivity and do not provide a valid estimate of vertical conductivities. Their conclusions regarding thermal anisotropy have been confirmed by others (Demongodin, Pinoteau et al., 1991; Deming, 1994; Midttomme and Roaldset, 1999; Revil, 2000). If a clay thermal conductivity of 1 mW/m-K is used in the GBRN (Luo, Wood et al., 1994) fabric model, rather than the commonly assumed mixed layer clay value of 1.85 mW/m-K, a shale of the composition cited above would have a

calculated thermal conductivity of 1.49, which is essentially identical to the Platte River value.

Based on this review we have considerable confidence that the lithologic end-member thermal conductivities listed in Table 2 are the good estimates. We use them in the Luo, Wood et al. (1994) fabric model to calculate the thermal conductivity of basin sediments that are a mix of sand, shale, carbonate, salt and water and a function of porosity and temperature.

Except for thermal conductivity and permeability, the material properties we use are linear combinations of the end-member values. Lithology is described by the volume fraction sand, shale, carbonate sand, carbonate mud, and salt in a computational finite element. Since our computational grid is attached to the solid sediment matrix, an element will commonly enclose a portion of a strata. The end-member properties of pure sand, shale, etc., are given in Table 2. The linearity of combinations of these end-member properties means, for example, that a 50% sand 50% shale mixture would have an uncompacted porosity of 0.37, a grain density of 2.76, and a rigidity of 1685 bars.

b. Porosity

Porosity is a linear function of effective stress to a minimum porosity, and sediment density is a linear function of porosity:

$$\begin{aligned} \phi &= \phi_o \frac{\sigma' - p_1}{\sigma_c} \quad , \text{ for } \phi \geq \phi_{\min} \\ \phi &= \phi_{\min} \quad , \text{ for } \phi \leq \phi_{\min} \end{aligned} \quad (2)$$

$$\rho_s = \rho_G(1 - \phi) + \rho_w \phi, \quad (3)$$

where σ' is the reduced lithologic stress (lithologic stress minus hydrostatic pore pressure), p_1 is the excess pore pressure (pore pressure minus hydrostatic pressure), ρ_w is the density of pore water, ρ_s the density of the basin sediment, and ρ_G and ϕ are the grain density and porosity of the sediment computed as linear combinations of the end-member lithology values given in Table 2. Porosity is not allowed to increase in our models. It might also be noted that the rigidities are about 50 times smaller than the rigidities used in reservoir engineering and hydrologic simulations of fluid flow. Over geologic times, mineral grains dissolve and/or deform where pressed together. This accounts for the greater compressibility. The compressibility is calibrated to Gulf of Mexico sediments in the Eugene Island Block 330 area (Coehlo, 1997).

c. Permeability

Permeability, k in millidarcies, is computed from the fraction coarse-grained sediments (e.g., the sum of the fraction sand and the fraction carbonate sand), f_{coarse} , and porosity of an element:

$$\begin{aligned} \log k &= (5f_{coarse} - 3) + 28.5f_{coarse}(\phi - 0.2) \\ f_{coarse} &\leq 0.7 \\ \log k &\leq 5 \end{aligned} \tag{4}$$

Equation (4) was deduced from Pennzoil core plug measurements (Coehlo, 1997). Depending on the lithologic fraction of coarse material (sand or carbonate sand), the permeabilities range from 1 microdarcy to 100 darcies. The lowest (1 microdarcy) permeability is not sufficient to allow overpressures to develop in a model basin. To produce overpressures, seals of very low (10^{-9} millidarcy) permeability are deliberately inserted in our models. This allows full control on the geometry and possibly time-dependent location of overpressured areas in a basin.

d. Radiogenic Heat Production

Radiogenic heat production in sedimentary rocks contributes significantly to basin surface heatflow. Blackwell and Steele (1989) pointed out, for example, that radiogenic heat in a thick sediment section can be a substantial fraction of the total normal heat flow. The same point is made by McKenna and Sharp (1998) who calculated the radiogenic heat production in Texas Gulf Coast sediments from their U, Th and K contents. In our modeling we assume shales and sands in our models have the K, U, and Th contents measured by McKenna and Sharp (1998) for the Frio mudstones and sandstones. The values we assume and the resulting heat generation per kilogram solids in Gulf Coast end-member lithologies are given in Table 3 below.

Table 3. Heat generation for Gulf of Mexico sediments. Data from McKenna and Sharp (1998). K, U, and Th indicate the potassium content of the sediments in wt%, and the uranium and thorium content in parts per million. A_T is the heat generation in nano-watts per kilogram. It is calculated from the K, U, and Th contents using conversion constants, C_o , as listed in Yalcin, Littke et al. (1997).

	K[Wt %]	U[ppm]	Th[ppm]	A_T[nW/kg]
C_o	0.0335	0.0979	0.0264	
Frio Sandstones	1.6	3.7	8.7	0.63
Frio Mudrocks	2.2	4	10.6	0.73
Stuart City ls	0.3	0.9	2.1	0.15
Salt	0	0	0	0

The heat generation parameters listed in Table 3 are appropriate estimates for the offshore Louisiana Gulf of Mexico, but it should be kept in mind that the radiogenic element content of sediments could vary with depth and distance from shore. If the radiogenic element content is as listed in Table 3, the heat flow from the thickest (>12 km) part of the Louisiana section could be as high as 20 mW/m^2 , or nearly all the measured heat flow from this area (see Figure 6). There can therefore be no question of the potential importance of radiogenic heat production if the radiogenic element concentrations of Gulf sediments are at all similar to those listed in Table 3. The values listed in Table 3 are typical of basins worldwide (Rybach, 1976; Keen and Lewis, 1982; Wollenberg and Smith, 1987).

3. Thermal Models

All our thermal models, whether 1D, 2D, or 3D, are finite element Galerkin models. The grid is attached to the material matrix, and elements deform as the sediments compact or are faulted. Transformation from Eulerian to material coordinates follows the methods of Palciauskas and Domenico (1989).

The calculation domain is the basin itself. Heat flow to the base of the section is specified by the plate model described above. The temperature at the top surface of the basin (the seafloor or land surface) is fixed according to the ambient air temperature if the basin surface is subaerial, or from the water depth relative to the thermocline if the basin surface is below sea level. In this later case the surface temperature is assumed to be T_{water} if the surface is above the top of the thermocline, D_{tmclt} , and $T_{\text{deepwater}}$ if the seafloor is below the bottom of the thermocline, D_{tmclb} . Surface temperatures are linearly interpolated between these two values if the seafloor lies between D_{tmclt} and D_{tmclb} . The values for these parameters we use in modeling the Louisiana section are given in Table 1.

Water depth in the past can be calculated from the present-day water depth, sediment thickness and isostasy, or can be determined from fauna and sediment characteristics. To apply the first method we compute the fraction of the load that is supported elastically by the lithosphere and then compute the isostatic subsidence produced by the remainder of the load. Water depth at a past time is computed by adding the present water depth to the sediment thickness deposited since the time of interest and subtracting the sum of the isostatic rise (due to unloading) and the rise due to decompaction of the underlying sediments. The isostatic rise is computed by Fourier transforming the load, filtering the high frequency components that are supported by the elastic lithosphere, and then retransforming and computing the isostatic subsidence on the filtered load. The flexural rigidity model used is described in Cathles (1975). In higher resolution models, the subsidence due to salt movement is added.

4. Chemical Modeling Methods

a. Hydrocarbon Maturation Models

To model the maturation of the Upper Jurassic Type II source we use a simplified version of a standard Burnham and Sweeney Type II model (Braun and Burnham, 1990) with a modified reaction stoichiometry for the breakdown of oil to gas. The stoichiometric matrix for the decomposition of kerogen to hydrocarbons and other products is shown in Table 4. The pre-exponentials and activation energies used in our models are those recommended in Burnham and Braun (1990). We have eliminated the breakdown reaction for CH_x because we believe this reaction will occur only at temperatures of 350°C or more. Light hydrocarbons are extremely difficult to crack (E. Colling, p.c., 2002). The reaction occurs at the high temperature limit of the anhydrous pyrolysis analyses, but only in the most extreme circumstances in basins. We modify the breakdown of cokable oil (through semicoke) so that about 50% char and 50% methane is produced, based on the assumption that the average composition of cokable oil is about

CH₂ and therefore that CH₂ → 0.5 C + 0.5 CH₄. We consider that 0.791 g of the total organic carbon is reactive. This enforces an overall HI of 0.65. The breakdown of Type II kerogen in the model summarized in Table 4 results initially in 0.65 g of liquid hydrocarbons (oil plus a little condensate and methane). The oil subsequently cracks to char₂ (28%), CH_x (39%) and CH₄ (33%), so that ultimately 1 g of TOC produces 0.27 g CH₄ and 0.27 g CH_x. The volume change associated with kerogen decomposition is calculated by summing the grams of product produced or destroyed divided by the densities listed in Table 4.

The oil generation rates agree with an industry standard compositional kerogen kinetic model for the Kimmeridge clay in the Weald Basin, U.K. The oil decomposition kinetic model is not constrained other than by the experimental data upon which it is based.

To model the maturation of the Eocene Type III sources we modified a Wilcox Coal Rock-Eval pyrolysis kinetic model contributed by industry by adding CO₂ generation and oil cracking as shown in Table 5. The CO₂ generation model uses kinetics suggested by John Hunt (p.c. 1991) and the OI index (70 mg/g) of the industry model. The oil decomposition parameters are the same as for the Type II model in Table 4.

Table 4. The maturation model for Type II kerogen used in our calculations is simplified from Braun and Burnham (1990) and Burnham and Braun (1990). The breakdown of oil to gas, condensate, and char is modified as discussed in the text. E* is the activation energy and σ is the Gaussian spread of up to 24 weights. If σ=0 there is a single activation energy with weight 1. We assume 0.791 g of the kerogen is reactive. One gram of TOC thus produces 0.168 g of cokable oil (= 0.213 × 0.791). The initial (oil stage) hydrogen index is thus 652 mg/g TOC of which 622 mg/g is oil and the rest CH_x and CH₄. The gas stage HI is 538 because the breakdown of oil to CH₄ precipitates solid product.

	ρ [g/cm ³]	Kerogen	Uncoke. Oil	Coke. oil	Semicoke	Char 1	Maximum Yields
Kerogen	1.5	-1	0	0	0	0	0.791
Uncokable oil	0.8	0.573	-1	0	0	0	0.4532
Cokable oil	0.8	0.213	0	-1	0	0	0.1685
Semicoke	0.6	0	0	0.95	-1	0	0.1601
Char 1	1.8	0.16	0.335	0	1	-1	0.4385
CH _x	0.7	0.036	0.530	0	0	0	0.2687
Char 2	1.8	0.0155	0.047	0	0	0.5	0.2528
CH ₄	0.6	0.0025	0.088	0.05	0	0.5	0.2695
Preexp[s ⁻¹]		2.4×10 ¹³	1×10 ¹²	0.3×10 ¹²	8×10 ¹²	3.2×10 ¹²	
E*[kcal/mole]		51	55	45	51	56.85	HI Oil Stg 0.652
Gaussian σ		1.53	0	0	0	6.82	HI Gas Stg 0.538

Table 5. The Type III maturation used to calculate the maturation of the Eocene source beds in the GRI Corridor. The model is based on Rock-Eval pyrolysis kinetics for the Wilcox Coal. CO₂ generation and oil cracking have been added as described in the text.

	ρ [g/cc]	$K0$	$K1$	$K2$	$K3$	$K4$	$C15+$	$C5-15$	$Max\ Yields$
K0	1.5	-1	0	0	0	0	0	0	0.070
K1	1.5	0	-1	0	0	0	0	0	0.062
K2	1.5	0	0	-1	0	0	0	0	0.082
K3	1.5	0	0	0	-1	0	0	0	0.030
K4	1.5	0	0	0	0	-1	0	0	0.030
C15+	0.8	0	1	0	0	0	-1	0	0.062
C5-15	0.7	0	0	1	0	0	0	-1	0.082
C2-4	44	0	0	0	1	0	0.5	0.2	0.078
C1	16	0	0	0	0	1	0.1	0.8	0.102
R1	1.2	0	0	0	0	0	0.4	0	0.025
CO ₂	44	1	0	0	0	0	0	0	0.070
PreExp[1/s]		7×10^4	Industry Wilcox Type III				10^{12}	10^{12}	HI _{Oil} = 0.204
E*[kcal]		32.2	parameters				55	55	HI _{Gas} = 0.179
σ		0					0	0	OI = 0.070

b. Hydrocarbon and Brine Migration Models

Brine migration is modeled by solving a finite element pressure equation. The driving force of fluid movements is compaction and positive-volume hydrocarbon maturation reactions. The base and sides of the basin are assigned no-flow boundary conditions. Flow is allowed out the top surface. A finite element solution to the pressure equation and Darcy's Law determines how pore waters flow from these sources to the surface through the sediment permeability distribution algorithmically computed as a function of porosity and lithology (described above). Brine flow is single phase.

Hydrocarbon migration is computed by propagator techniques that track how the hydrocarbons generated in source strata elements will move into and saturate adjacent finite elements. Mobile maturation products are expelled when their volume exceeds an expulsion fraction of the source strata porosity, S_{Expul} . In all our modeling we take $S_{Expul} = 0.2$ of the pore space.

Once expelled from source beds, hydrocarbons are allowed to move from one element to the next when a migration pore saturation, S_{Migr} , is exceeded. The migrating hydrocarbons are allowed to mature by conversion of oil to gas components as they migrate. The migration pore saturation is treated as a parametric variable in our modeling. It is much less than S_{Expul} , typically having a value of $\sim 0.025\%$ (e.g., 0.125% of the pore space in a finite volume has 20% hydrocarbon saturation).

The migration of hydrocarbons may be parallel to the brine flow computed by the finite element model, or vertical (driven by pure buoyancy), or any vector rotation between these two extremes. At any timestep the composition of mobile (hydrocarbon) products in an element is determined by mixing the products already present with those introduced before the excess product is moved to the next element. In this fashion, the changing chemistry of the migrating (hydrocarbon) product column is predicted.

D. Modeling Results

1. A 1050 km Long Section Across the Entire Offshore Louisiana Basin

Water depth, heat flow history, and sediment properties are best defined considering the entire basin. We model the 1050 km long section discussed in Volume II of this report series shown in Figure 1. Figure 1 depicts model lithology in the Louisiana Section. Lithology (mainly a mix of sand and shale) is based largely on the information contributed by Exxon. The basin is mostly shale, but sand contents range to 65% beneath present-day Louisiana, and turbidite sand deposition at the base of the slope increases the sand content there.

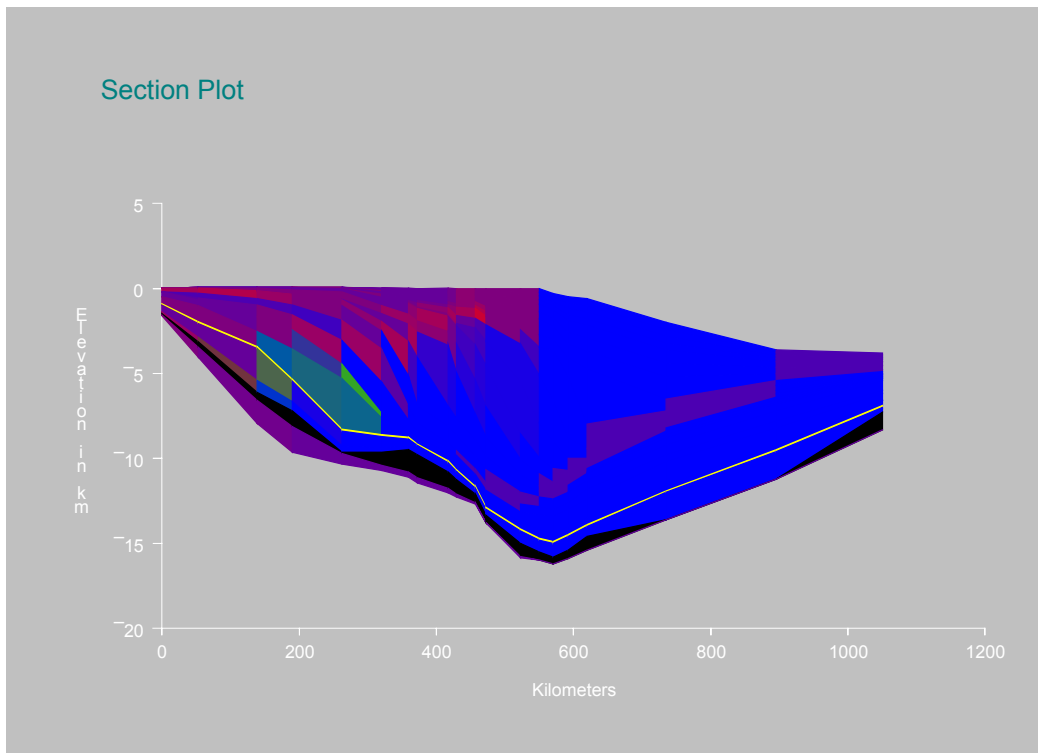
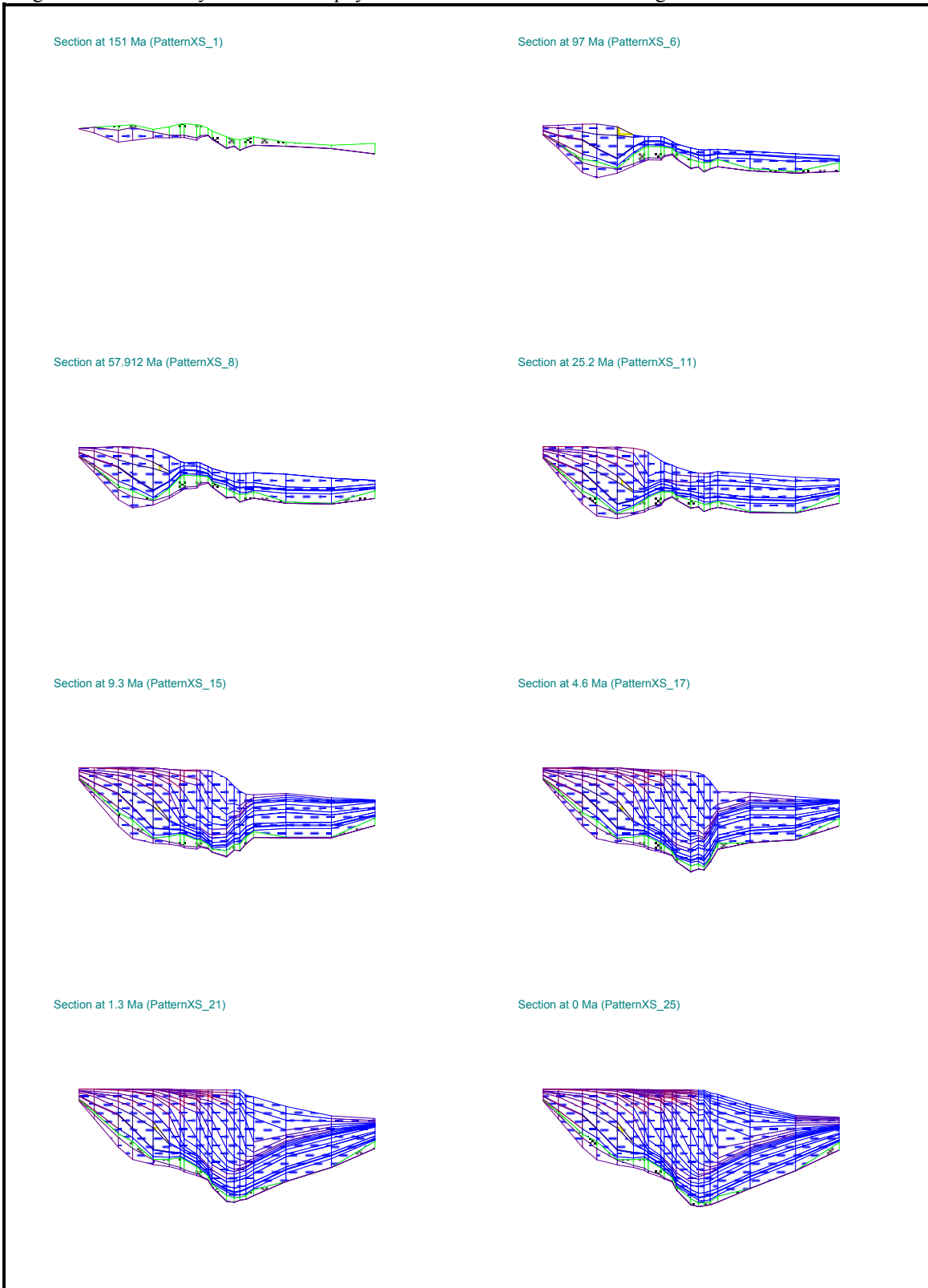


Figure 1. A finite-element model of a present-day N-S section through central Louisiana from the Arkansas border to deep water Gulf of Mexico. Color indicates lithology as determined by Exxon: blue is shale, red is sand, and green is carbonate. The thin yellow line indicates the 100 m thick Jurassic source rock used in modeling. Preparation of the section is described in Volume II of this report series. North is to the left.

a. Physical Evolution of the 1050 km Section

The physical evolution of the Louisiana section is shown in Figure 2. This physical evolution was computed by backstripping, decompacting, thermal cooling, and inferring sea level change since rifting at 158 Ma, as discussed above. The scale of Figure 2 can be inferred from Figure 1, which corresponds to the last image in Figure 2. The water depth increases from about 2.5 km at the south end of the section at 151 Ma to the present depth of ~3.8 km. The increase in water depth is due to the post-rifting cooling and thermal contraction of the lithosphere, but this is offset by the deposition of sediments even at the far southern end of the section.

Figure 2. Numerically reconstructed physical evolution of the section in Figure 1.



b. Thermal Evolution

The ratio of the pre-rift lithosphere thickness to the lithosphere thickness immediately after rifting is defined as $\beta(x)$ where x is the distance along section shown in Figure 1. $\beta(x)$ is inferred from the present-day water depth and the present-day thickness of the accumulated sediments using equation (1). Heat flow in the base of the section is then predicted from β , heat generation in the crust, heat generation in basin sediments, and the sedimentation rate using the lithosphere-scale (150 km thick) plate model described above. The predicted heat flow in the base of the section (top of basement) and at the top surface of the basin is shown in Figure 3. Shallow heat flow measurements from Figure 14 of Volume II are plotted as squares.

The model surface heat flow compares very well with that observed, except at the far north end, where the observed values range from 50 to 88 mW/m² (or 1.2 to 2.1 HFU) (Smith and Dees, 1982), and at ~500 km along the section. Land heat flows can be affected by fluid flow and other phenomena, and the values in the middle part of the section are projected from off-section measurements. Overall the agreement between the model and observed surface heat flow is remarkably good, especially considering that we have used literature values for all parameters. The calculations show that the very low heat flow values in the middle of the section are caused by the rapid sedimentation.

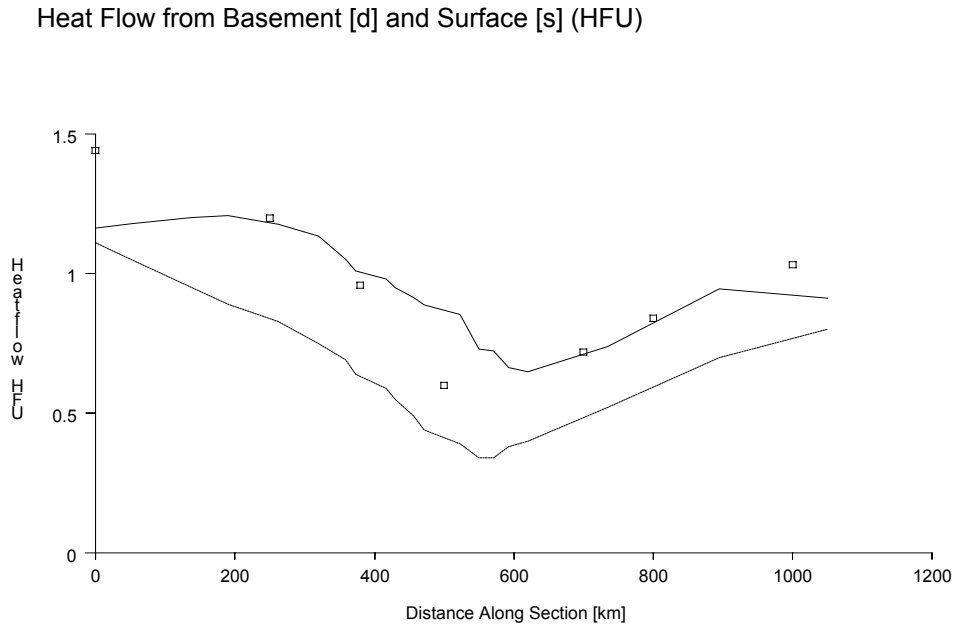
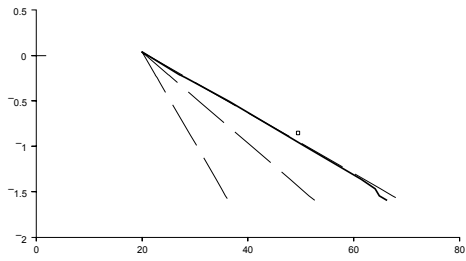
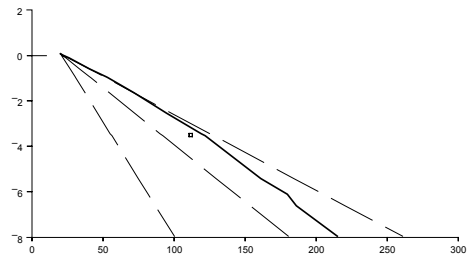


Figure 3. Present-day heat flow in the base of the sedimentary section (bottom curve) and from the top surface (top curve) of the basin predicted by the plate model described in the text. Radiogenic heat production is included in the basin sediments and is responsible for the difference between the upper and lower curves. The low heat flows in the middle portions of the section are due to the rapid sedimentation rates there. The observed heat flow along the section (from Figure 3 of Volume II) is plotted as square symbols.

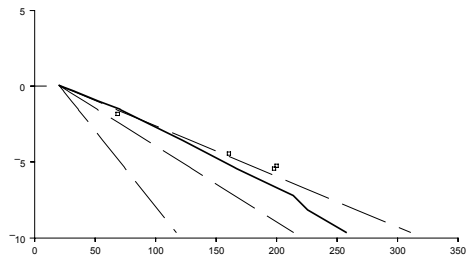
T[Z] Fed_Royalty_1 (T Well 1)



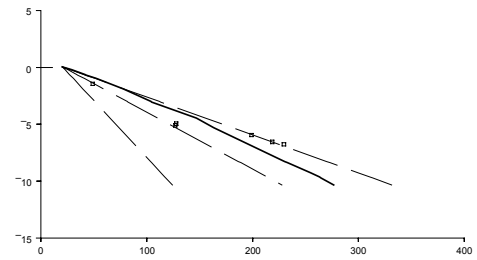
T[Z] Arkla_1 (T Well 3)



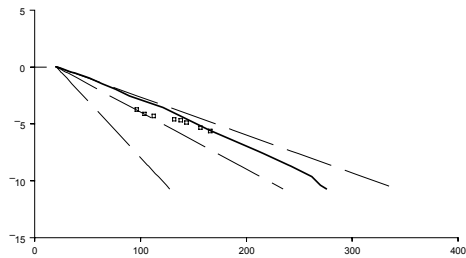
T[Z] Ameranda_1 (T Well 4)



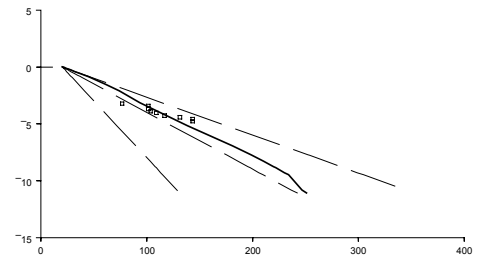
T[Z] Hunt_1 (T Well 5)



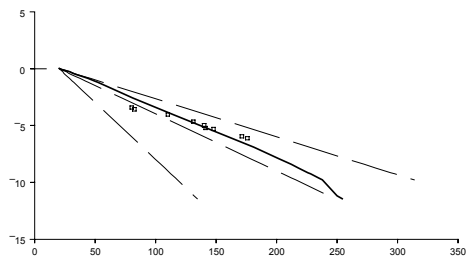
T[Z] Amer_Q_1 (T Well 6)



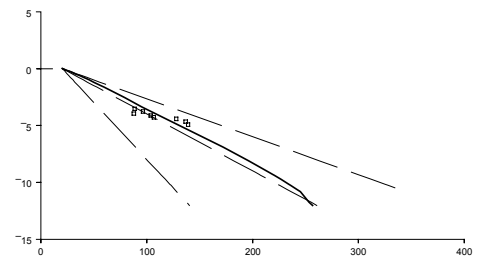
T[Z] Shell_1 (T Well 7)



T[Z] Ameranda_1 (T Well 8)



T[Z] McDermott_2 (T Well 9)



Temperature in °C

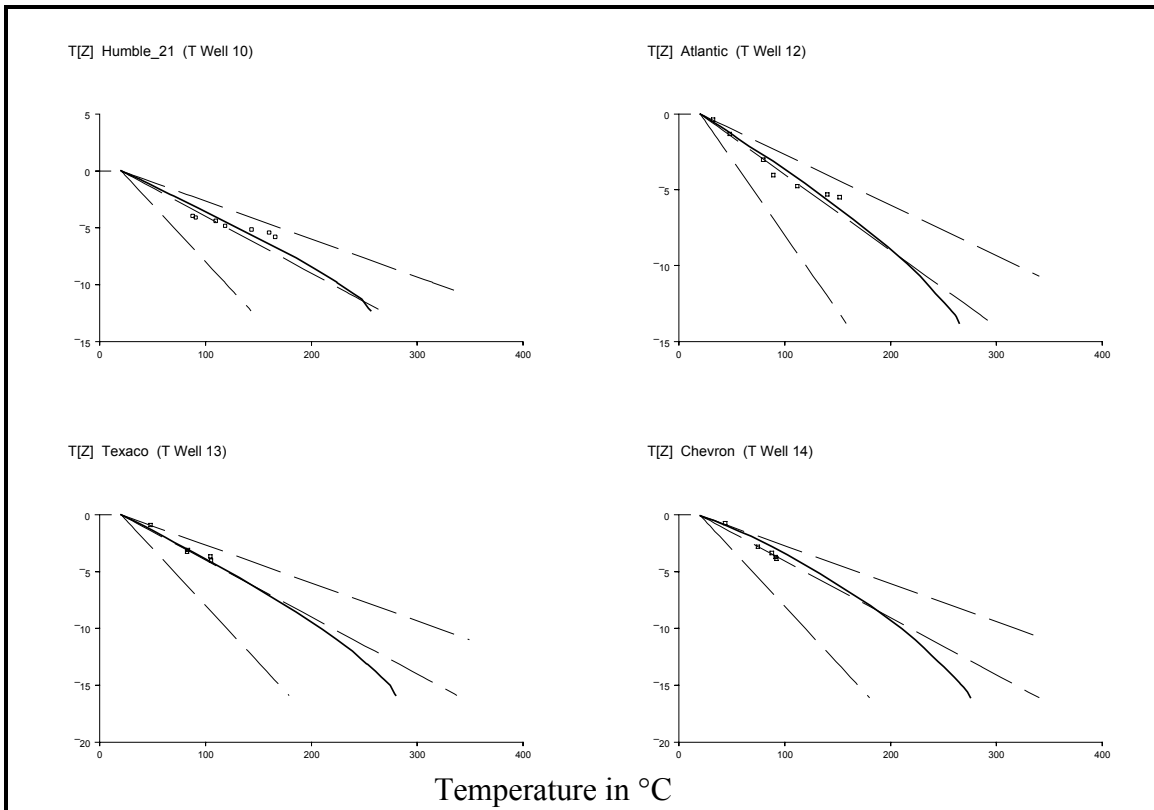


Figure 4. Comparison of model and observed temperatures in all wells where we have temperature data along the Louisiana Section (Figure 1). The vertical axis is elevation in km above present sea level. The dashed lines indicate temperature gradients of 10, 20 and 30°C/km. The solid line is the temperature profile predicted by the model. The points are measured bottom hole temperatures provided by Exxon to the GBRN. The temperature gradients decrease from 30°C/km in the north to 20°C/km in the southern parts of the section.

Figures 4 and 5 compare the observed subsurface temperatures and vitrinite reflectance measurements to values predicted by the model. The subsurface temperature gradient decreases along the section from 30°C/km in the north to 20°C/km in the south.

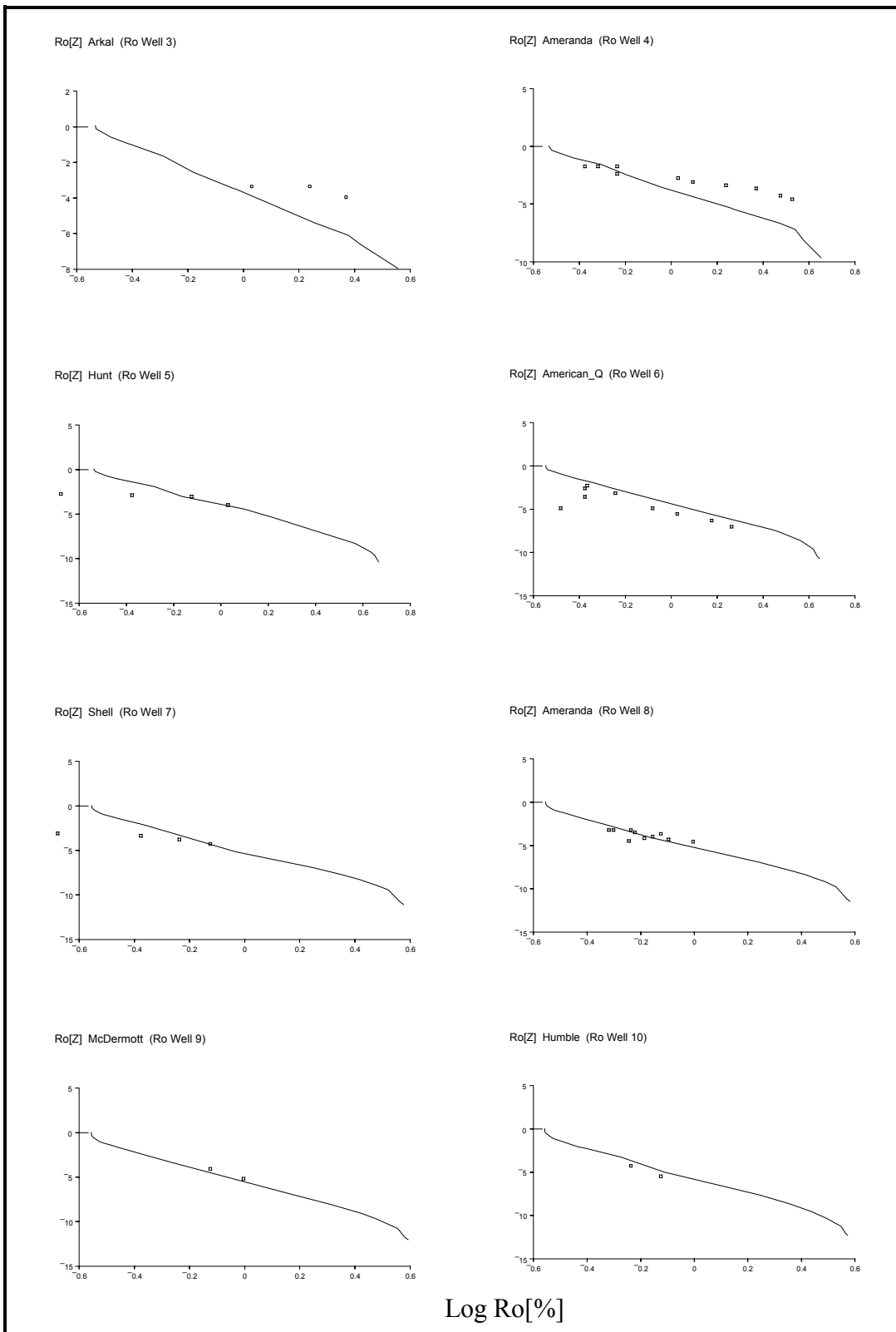


Figure 5. Comparison of vitrinite reflectance profiles calculated using the kinetic model of Burnham and Sweeney and measured values provided by Exxon. The vertical axis is elevation above present sea level.

c. Discussion

The model heat flows and subsurface temperature gradients match those observed remarkably well, especially considering that we have used parameters from the literature that are not adjusted to fit local conditions. The predicted subsurface temperatures agree with those observed, especially well in the GRI Corridor, which spans from well 12 to midway between well 17 and 18 of the Louisiana Section (see Figure 6 and Figure 3 in Volume II). Figure 4 shows that the subsurface temperature gradients are $\sim 20^{\circ}\text{C}/\text{km}$ as observed in the Corridor. Figure 5 shows that the vitrinite R_o values computed for the model time-temperature history match those measured very well. This agreement-without-tuning between model predictions and observations provides considerable confidence that the heat flow history and the temperature histories of the basin are well simulated by the model.

2. A 200 km 2D N-S Line Across the GRI Corridor

a. Transfer of Louisiana Section Boundary Conditions

The heat flow history defined by the 1050 km Louisiana line model (and the 1D plate modeling that provided input to it) is transferred to a 200 km long 2D north-south section across the Corridor as shown in Figure 6. The geology in this section is a stretched version of a section published by McBride (1998) that lies ~ 50 km to the east of the Corridor. McBride's section provides the only published estimate of the depth to the Jurassic and Eocene strata and gives the best salt distribution. This is discussed in Volume II of this series.

The critical inputs to the 200 km line include heat flow to the base of the sediment section and the water depth (which specifies the temperature of the sediment-water interface). Heat flow is taken from the 1050 km long Louisiana Line as indicated in Table 6. Water depth over the last 13.4 Ma was determined assuming water depths relative to the shelf were the same in the past as at present. The position of the shelf edge was taken from Winker (1982), and Galloway, Ganey-Curry et al. (2000) following Cornelius, Cathles et al. (accepted). Before 13.4 Ma water depths were taken from the Louisiana Line model.

The geologic history of the 200 km section shown in Figure 6 was determined using the methods described above. The resulting geologic history is shown in Figure 7. Reconstruction begins at 144 Ma. The first image shows the deposition of the Louann salt when the water depth was ~ 4 km. Deposition of carbonates (yellow) and clastics (red for sand and blue for shale) is relatively uniform to 10.5 Ma at which time the Louann salt inverts to form a near-surface sill. We do not show the decreased thickness of the Louann that would have occurred at this time in our models. Because it is below the Jurassic source, changes in thickness of the Louann salt do not affect our calculations. Sediment deposition on the salt sill produces salt withdrawal minibasins, first in the northern half of the section (filled by 5.8 Ma) and then in the southern half (filled by 1.4 Ma).

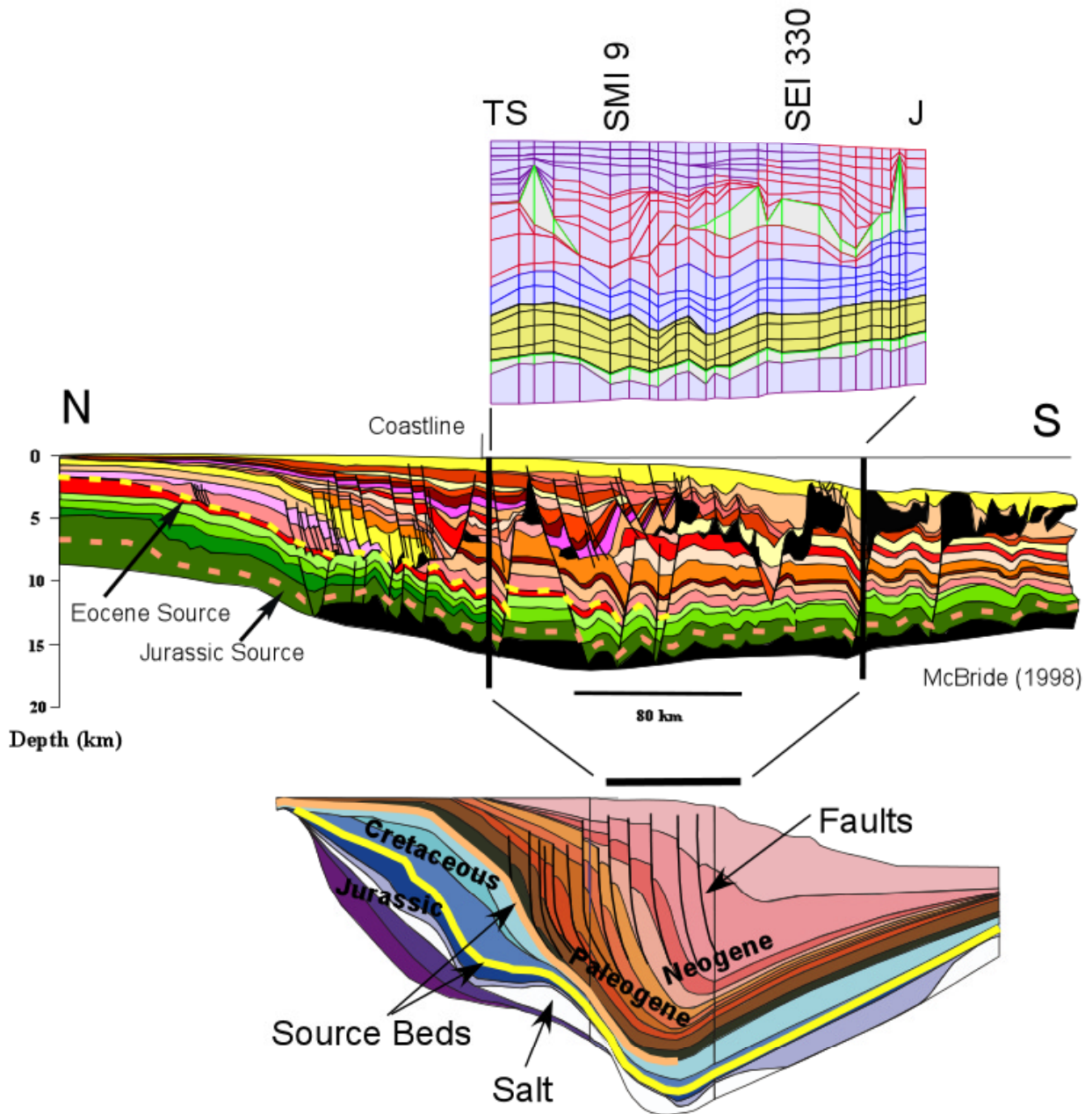


Figure 6. Extraction of a 2D Corridor Model from the Louisiana Line. The geology in the extracted GRI Corridor is taken from a section published by McBride that lies ~50 km east of the Corridor. Salt is indicated in green, carbonate sediments in yellow, shales in blue, and sandy shales in red. The model Jurassic and Eocene source beds lie at the bottom and top of the carbonate (yellow) layer. The Eocene source extends only half way across the section. Colors in the Louisiana Section depict stratigraphic age. The Corridor is ~125 km E-W and ~200 km N-S.

Table 6. Heat flow as a function of time for the 9 pseudowells in the 1050 km section (Figure 1) that define the Corridor. The left column gives the ages of the strata in the model. The heat flows are those that apply at the time these strata were at the surface and are the heatflows into the base of the basin. Radiogenic heat production is assigned to the sediments as specified in Table 1.

Age[Ma]	Hbl	Tx	Atl	Tx	Chev	15	16	17	EndCor
0	0.59	0.55	0.52	0.49	0.46	0.46	0.5	0.51	0.51
0.325	0.59	0.55	0.52	0.49	0.46	0.47	0.5	0.51	0.51
0.65	0.59	0.55	0.52	0.49	0.47	0.47	0.5	0.52	0.52
0.975	0.59	0.55	0.52	0.49	0.47	0.47	0.5	0.52	0.52
1.3	0.59	0.55	0.52	0.5	0.47	0.48	0.51	0.53	0.53
1.95	0.6	0.55	0.52	0.5	0.48	0.48	0.51	0.54	0.54
2.6	0.6	0.56	0.53	0.51	0.49	0.49	0.52	0.55	0.55
3.8	0.6	0.56	0.53	0.51	0.5	0.51	0.55	0.63	0.63
4.6	0.61	0.56	0.53	0.52	0.51	0.54	0.57	0.66	0.66
6.3	0.61	0.56	0.53	0.53	0.54	0.59	0.69	0.76	0.76
9.3	0.61	0.56	0.54	0.58	0.64	0.69	0.76	0.81	0.81
14.8	0.57	0.57	0.58	0.68	0.73	0.77	0.81	0.83	0.83
16.5	0.61	0.65	0.67	0.77	0.81	0.84	0.84	0.86	0.86
20	0.68	0.74	0.78	0.85	0.87	0.88	0.88	0.88	0.88
25.2	0.86	0.86	0.87	0.9	0.91	0.9	0.9	0.9	0.9
33	0.95	0.95	0.95	0.95	0.95	0.95	0.95	0.94	0.94
49.5	1.07	1.06	1.05	1.04	1.03	1.03	1.03	1.02	1.02
57.9	1.15	1.15	1.14	1.13	1.12	1.11	1.11	1.11	1.11
59	1.15	1.15	1.14	1.13	1.12	1.11	1.11	1.11	1.11
97	1.46	1.48	1.47	1.47	1.46	1.45	1.45	1.47	1.47
112	1.66	1.69	1.68	1.67	1.66	1.65	1.65	1.67	1.67
127.7	2.1	2.14	2.14	2.11	2.11	2.09	2.08	2.11	2.11
131	2.27	2.33	2.33	2.29	2.29	2.26	2.25	2.28	2.28
144	3.37	3.48	3.51	3.32	3.38	3.43	3.47	3.47	3.47
151	3.96	4.56	4.43	4.24	4.48	4.29	4.4	4.43	4.43
158	1.78	1.79	1.79	1.78	1.79	1.78	1.79	1.79	1.79
190	1.78	1.79	1.79	1.78	1.79	1.78	1.79	1.79	1.79

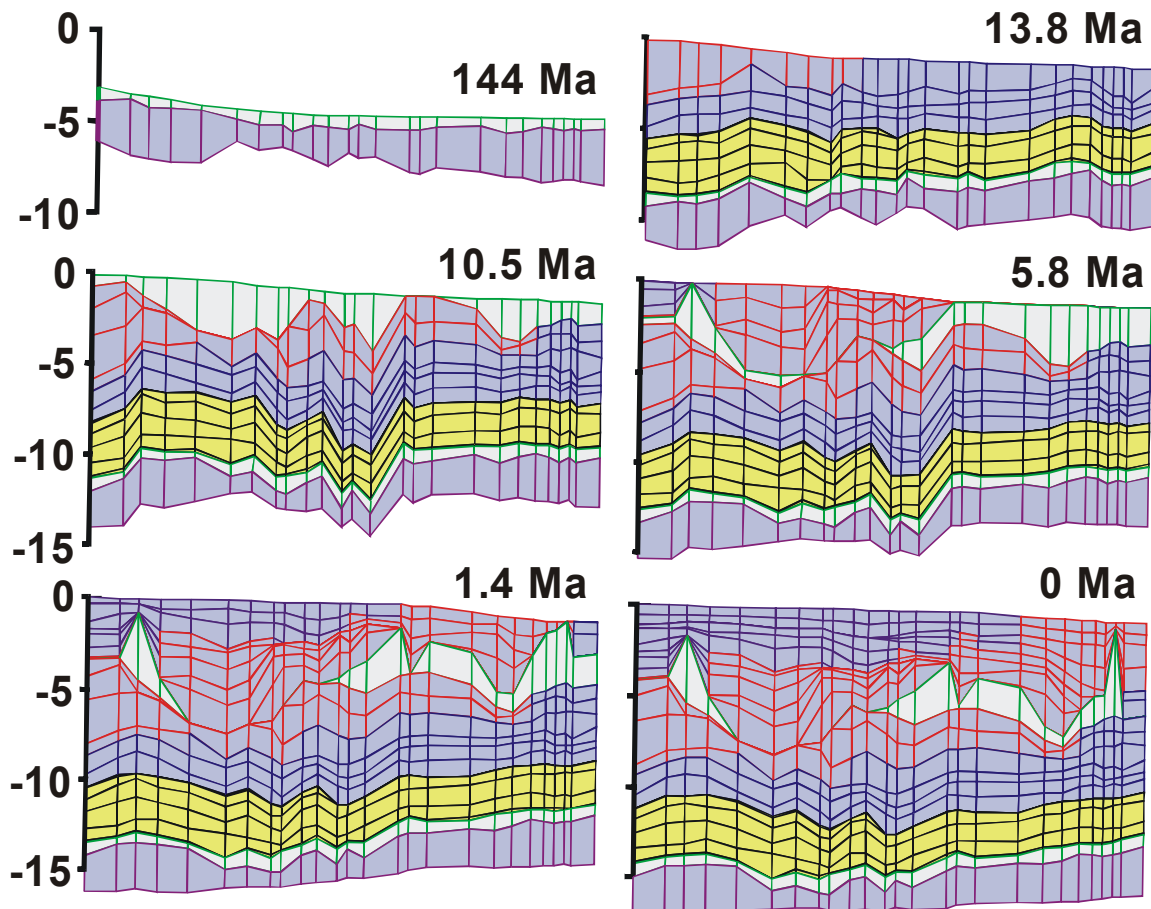


Figure 7. Geologic evolution of the McBride section, stretched to span the GRI Corridor as shown in Figure 6.

b. Geochemical Constraints: Gas Washing, Oleanane and Sulfur

Our analysis of 116 oils and 17 gases in the GRI Corridor is discussed in detail in Volumes III and IV in this series. The geochemical trends that are most significant for constraining models are: (1) a systematic decrease to the south in the intensity of what we call “gas washing” shown in Figure 8, and (2) a systematic decrease in the oleanane content and a rise in the sulfur content of oils to the south as shown in Figure 9.

The gas washing is dramatic. Over 90 wt% of the alkanes (and probably about the same wt% of the total oil) has been dissolved and carried away by gas in the Tiger Shoals area. From equation of state modeling we believe ~3.5 kg dry gas per kg oil (Meulbroek, 1997; Meulbroek, 1998) must be available at an appropriate time for washing to take place.

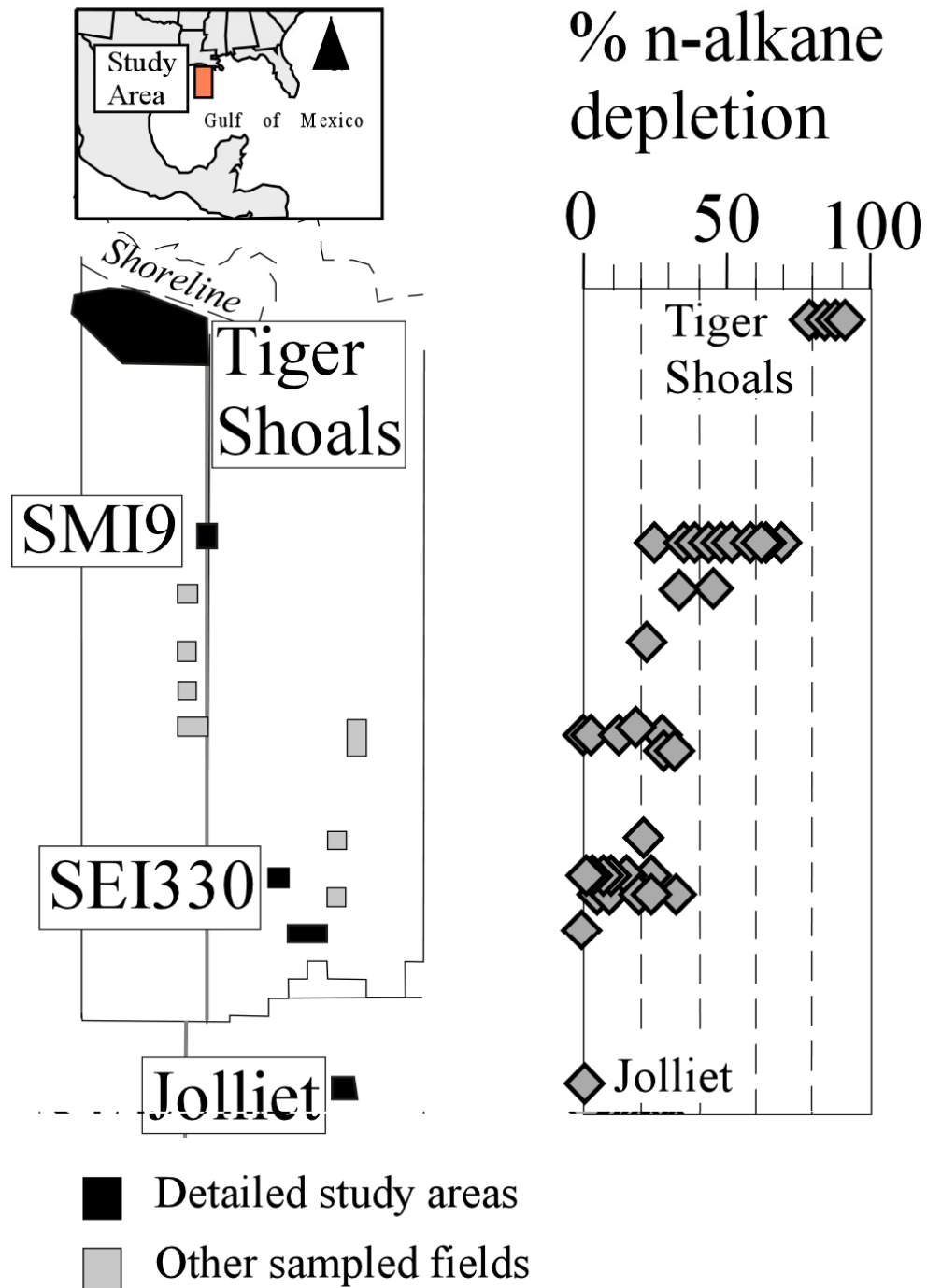


Figure 8. Oils in the northern part of the Corridor are severely depleted in light (<C23) end n-alkanes. By weight over 90% of the n-alkanes have been removed, we believe by gas washing. The intensity of gas washing decreases to the south across the Corridor.

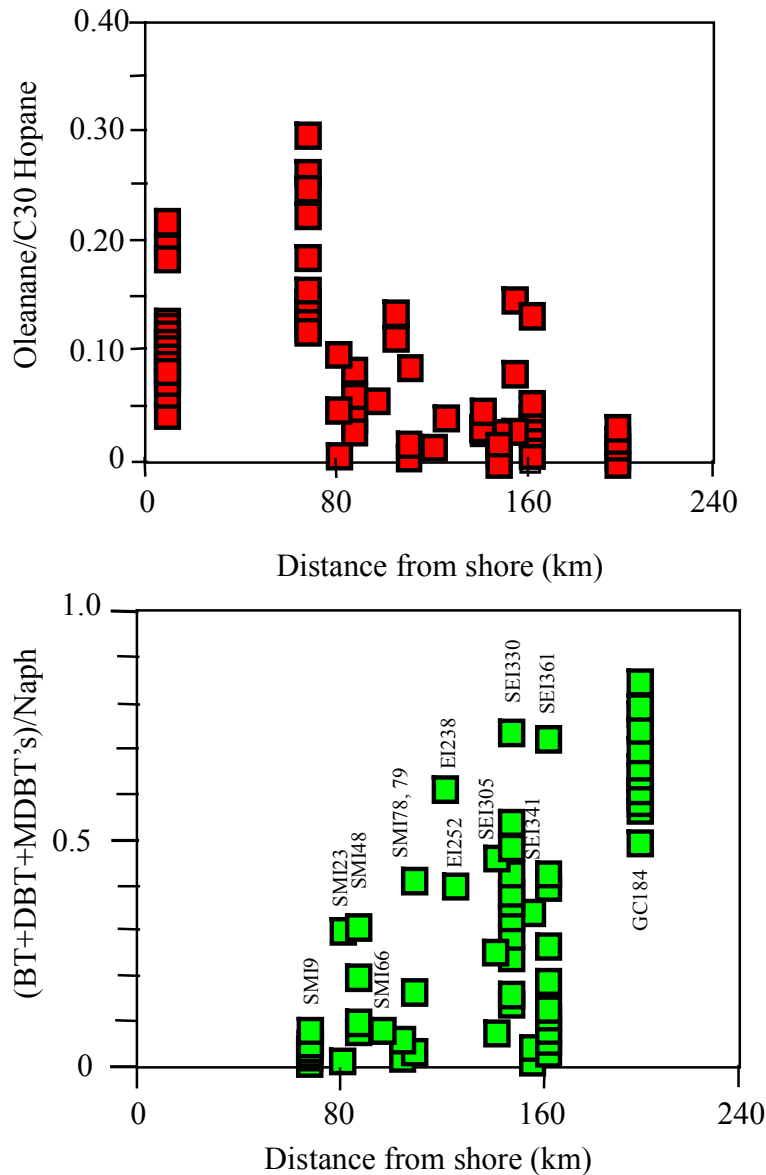


Figure 9. The decrease in oleanane to C30 hopane ratio to the south suggests a decreased contribution of oleanane-bearing Eocene-sourced hydrocarbons. An increase in sulfur-bearing benzothiophenes (BT+DBT+MDBT) to the south suggests an increase in marine Jurassic-sourced hydrocarbons.

The decrease in the oleanane-to-C30 hopane ratio and the increase in sulfur-bearing benzothiophenes (BT+DBT+MDBT) relative to naphthalene (Figure 9) suggest a decreasing contribution of Eocene-sourced hydrocarbons and an increasing contribution of Jurassic-sourced hydrocarbons to the south.

We will analyze 4 sites within the GRI Corridor in detail. The proven hydrocarbon resources at these four sites (equal to about 20% of the total in the Corridor) are summarized in Table 7.

Table 7. Proven hydrocarbon resources at four sites from Volume II in this series. See Figures 6 and 8 for the geographic locations.

	Oil (Condensate)	Gas	Oil+Gas [10⁹ t] (GOR)	Reservoir Age [Ma]	Res. Dpth [kmsf]	Est. filling time [Ma]	Bacterial Degrad.
Tiger Shoals	133x10 ⁶ bbls (46x10 ⁶) bbls 17.4x10 ⁶ t (0.6x10 ⁶ t)	6.4 TCF 129x10 ⁶ t	0.152 (5.7)	6 to 16.5	2.6 to 5.5	3.6 to 6.7	None
SMI 9	14.4x10 ⁶ bbls 1.9x10 ⁶ t	0.14 TCF 2.7x10 ⁶ t	0.0046 (1.42)	?	2.6 to 5.7	1	None
SEI 330	307x10 ⁶ bbls 40x10 ⁶ t	1.5 TCF 30x10 ⁶ t	0.071 (0.75)	0.9 to 1.8	1.4 to 2.4	0.23 to 0.1	Mod shallow, none deep
Jolliet	34x10 ⁶ bbls 4.4x10 ⁶ t	0.16 TCF 3.1x10 ⁶ t	0.0077 (0.71)	0.6 to 1.8	1.2 to 2.4	0.005	3 pulses refilling

c. Hydrocarbon Generation Potential

The Jurassic and Eocene source beds defined in Tables 4 and 5 could generate many times more hydrocarbons than are reseroired in the Corridor. This is most convincingly demonstrated by simple back-of-the-envelope calculations. Such calculations are summarized in Table 8 and discussed below.

The source beds are both deep enough that they are compacted in our model to the irreducible porosity of 10% and have a bulk sediment density of 2.48 g/cm³. The source bed kerogen total organic carbon content is discussed in Volume II. The initial kerogen mass in the source layers is estimated here from their thickness and aerial extent (a 200 km N-S section across the 200 x 125 km Corridor is shown in Figure 6). For example, the total mass of Jurassic kerogen in the GRI Corridor is 313 billion tonnes [(0.05 g Ker/g sediment) × (2.48 g sediment/cm³) × (0.1 km strata thickness) × (25,230 km² area of corridor, see Table 2 of Volume II) × (10¹⁵ cm³/km³) = 313 x 10¹⁵ g]. The mass of kerogen in the Eocene source is less (34 Bt) because that source extends only ~93 km across the Corridor, is 30 m rather than 100 m thick, and we assume the TOC content is 4 wt% rather than 5 wt%.

The hydrogen indices (HI) from Tables 4 and 5 provide a measure of the hydrocarbon generation potential of this kerogen. The hydrogen index is the mass fraction of hydrocarbon that would be produced if the total organic carbon (TOC) in a strata were fully matured. Because the breakdown of oil to methane precipitates solid product for the Jurassic maturation kinetics, the HI at the gas stage is less (0.54) than at the oil stage (0.652) of maturation. The HI of Eocene source is higher at the oil stage (0.204) than at the gas stage (0.179) for the same reason. The hydrogen indices multiplied by the TOC of the source strata give the hydrocarbon generation potential of Jurassic and Eocene source beds in the GRI Corridor. For the Jurassic source the hydrocarbon generation potential is 204 Bt at the oil stage and 168 Bt at the gas stage of maturation. The Eocene

hydrocarbon source potential is 6.9 Bt at the oil stage and 6 Bt at the gas stage of maturation.

The oil and gas must be expelled from the source strata to enter reservoirs. The 8th line in Table 8 estimates the amount of hydrocarbons that will be retained in the source beds if a hydrocarbon saturation of 20 vol% is required for their expulsion, and the density of the hydrocarbons is 0.6 g/cc. Because of the great pressures involved, a density of 0.6 g/cc is reasonable for even relatively pure methane gas. On this basis the retained hydrocarbon volume of the Jurassic source equals 30 billion tonnes = (0.1 km source bed thickness) × (0.1 porosity) × (0.2 expulsion pore fraction) × (0.6 g/cc hydrocarbon density) × (25,230 km² aerial extent of source bed). On the same basis, the Eocene source is capable of retaining ~4 Bt, but some of this retention will be CO₂. We estimate the expelled potential by multiplying the expelled hydrocarbon and CO₂ by the fraction of hydrocarbon.

The next to last row of Table 8 shows that the expelled hydrocarbon potential of the corridor is between 141 and 177 billion tonnes of hydrocarbon. This is over 100 times the 1.37 Bt of economically recoverable hydrocarbons that have been proven to exist in the Corridor. Since both source rocks are presently deeply buried and nearly fully matured (as we will see), we can conclude that the mobile hydrocarbons that have been discovered in the Corridor subsurface are but a tiny fraction of those that have been generated and expelled from the source rock.

d. Hydrocarbon Maturation, Migration, and Venting

Hydrocarbon maturation and migration were simulated for the 200 km section across the GRI Corridor shown in Figure 6, subject to the basal heat flows in Table 6. The hydrocarbons were expelled from the source strata when they occupied more than 20% of the pore volume of the source strata, and allowed to move from element to element in the overlying stratigraphy when more than 0.05% of the pore space in an element was filled with migrating hydrocarbon. The composition of the hydrocarbons in an element is determined by mixing the mobile hydrocarbon products introduced with products already present. The volume excess is then moved to the next element. Migration is vertical. The migrating hydrocarbons were further matured as they migrated as governed by the kinetics of Tables 4 and 5.

Table 8. The likely hydrocarbon source characteristics in the area shown in Figure 1 are synthesized from Gross, Hook et al. (1995), and Colling, Alexander et al. (2001). The Eocene source underlies only the northern ~half of the area. The generation potential is calculated according to the HI indices shown. The HI for the Jurassic source rock is from standard (Braun and Burnham, 1990; Burnham and Braun, 1990) kinetic models for Type II kerogen maturation (see Table 4). The Eocene HI are based on Rock-Eval pyrolysis of the Wilcox Coal as discussed in the caption of Table 5. Last row of table gives discovered hydrocarbon resources in the Louisiana Corridor (= recovered to date plus proven reserves = R_c). Data is from Bascle, Nixon et al. (2001).

	Jurassic Type II Source		Eocene Type II/III Source	
Bed Thickness [m]	100		30	
Aerial Extent in Corridor [km²]	125 × 201.8 = 25,230		125 × 93 = 11,630	
TOC [wt%]	5		4	
	Oil Stage	Gas Stage	Oil Stage	Gas Stage
Initial Kerogen Mass [Bt]	313	313	34	34
HI Index [g HC/gTOC]	0.652	0.538	0.204	0.179
Generation Potential [Bt]	204 (195 oil)	168	6.9 (+ 2.4 CO ₂)	6 (+ 2.4 CO ₂)
Source Retentn, $S_{HC}=20\%$ [Bt]	30	30	4	4
Expulsion Potential [Bt]	174	138	3.5	3.4
Corridor Discovered Resources, R_c	1.37 Bt hydrocarbons (0.46 Bt oil, 0.91 Bt gas) 11.1 × 10 ⁹ boe (2.62 Bbls oil, 45 TCF gas)			

As a check on chemical mass balance, the masses of all hydrocarbons (solid and fluid) were summed and plotted as a function of time. This is shown in Figure 10. The figure shows that 241 Bt of reactive kerogen is deposited in the basin between 144 and 138 Ma, and an additional 9.6 Bt are deposited between 53 and 50 Ma. This reflects the deposition of the source beds. The 241 Bt of reactive Jurassic kerogen equals 0.791×305 , where 305 Bt is the total Jurassic Type II organic carbon mass in the Corridor. This figure is slightly less than the 313 Bt estimated in Table 8. The factor of 0.791 is the fraction of the Jurassic kerogen that reacts to generate hydrocarbons (Table 4). Similarly the 9.6 Bt of reactive Eocene kerogen equals the total Eocene Kerogen in the Corridor (34.9 Bt) times the fraction of that kerogen that reacts to produce hydrocarbons or CO₂ (= sum of yields of K0-K4 in Table 5 = 0.274). The kerogens begin to mature to hydrocarbon and non-hydrocarbon products starting at ~30 Ma. The mobile products migrate vertically when the migration saturation of 0.05% is exceeded. Slightly more than half of the products (133 Bt which includes 2.4 Bt of CO₂) vent from the basin into the overlying ocean. The rest stay within the basin. The calculated total mass of hydrocarbon remains at 250 Bt showing that no hydrocarbons are lost in the numerical migration routines.

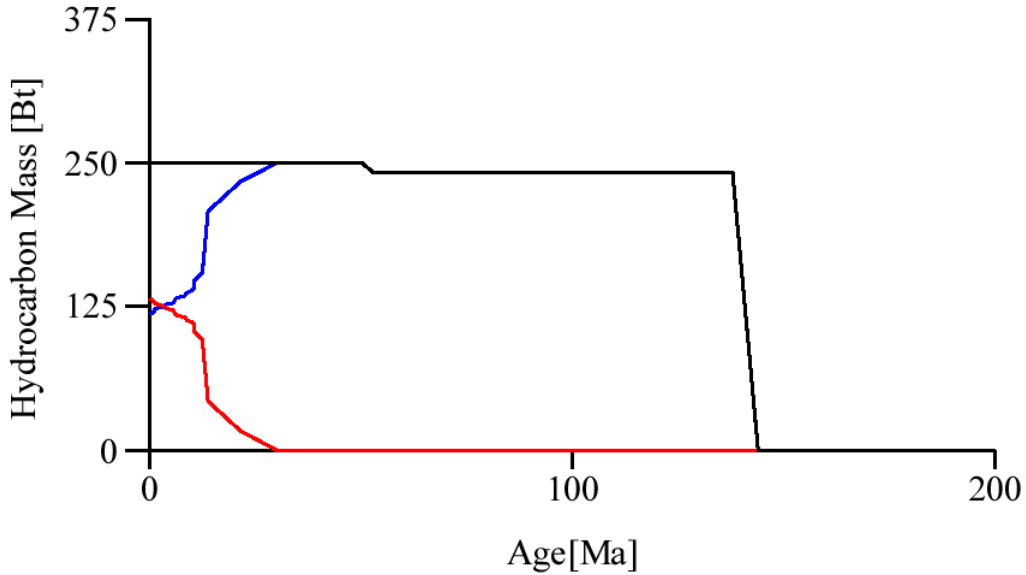


Figure 10. Mass balance of reactable organic carbon in GRI Corridor maturation/migration simulation. The top curve shows the total reactive kerogen mass deposited in the corridor as a function of time. It is the sum of the hydrocarbon mass vented to the oceanic (lower curve) and the hydrocarbon mass remaining in the basin (line departing from the top curve at ~30 Ma). The mass vented includes 2.4 Bt of CO₂ from the maturation of Eocene kerogen.

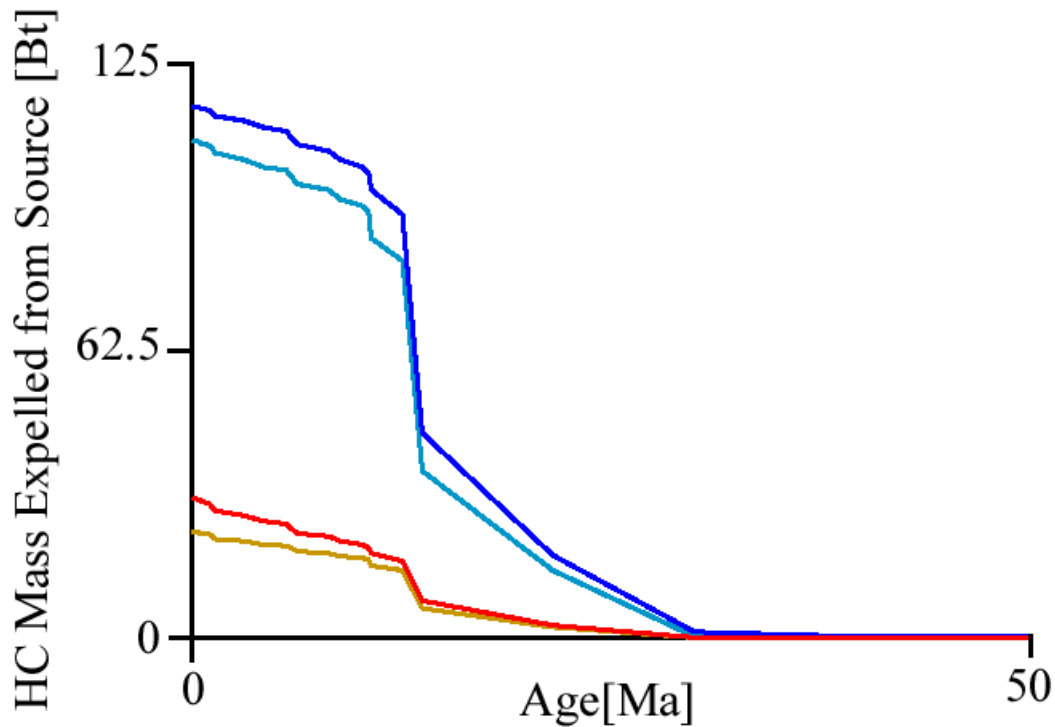


Figure 11. Total and vented masses of mobile hydrocarbons that have been expelled from their source rock in the GRI Corridor plotted as a function of time. The upper pair of curves is total and vented oil and the lower pair of curves is the total and vented gas. The total curves (which sum at 0 Ma to 147 Bt) represent the total oil and gas expelled from the source beds. The vented curves show that 131.5 Bt of hydrocarbon has vented into the ocean. The difference (15.5 Bt) is the mass of hydrocarbon retained within the migration conduits of the Corridor. Migration is vertical. The migration pore saturation, $S_{migr}=0.05\%$.

Figure 11 plots as a function of time, the mass of mobile hydrocarbon that has been generated and expelled from source strata, according to our model calculations. The figure also plots the hydrocarbon mass that has vented into the ocean. Because the migration saturation is very low (0.05% of the pore space), most of the hydrocarbons that are expelled from the source strata vent into the ocean. Of the 184 Bt of hydrocarbons that are generated in the Corridor model, 37 Bt are retained in the source strata, 15 Bt are retained in the migration pathways, and 131 Bt vent into the ocean. Almost all the kerogen has reacted (only 2.8 Bt have not), but 62 Bt of new solid products have precipitated in the Corridor.

The hydrocarbon discharge into the ocean is massive. This can be appreciated when it is realized that 131 Bt of hydrocarbon is equivalent to over 1000 billion barrels of oil, which is more than has been produced and consumed by humans since the start of the petroleum era. Table 9 summarizes these present-day statistics. Oil generation is essentially fully complete, but gas generation from solid and liquid products is continuing at the present day.

Table 9. Distribution of mobile and non-mobile hydrocarbons in the model GRI Corridor at the present day in billions of tonnes.

	Oil	Gas	Total Mob. HC	CO₂	Unreactd Kerogen	Precip Solids	Total
Vented	108.2	23.0	131.3	1.75			133.1
In Source Strata	12.6	24.6	37.2	0.7	2.8	61.9	117.7
Migrating	7.6	7.4	15.0				
Total	128.5	55.1	183.6	2.4	2.8	61.9	250.8

e. Computed Hydrocarbon Chemistry

Figures 12 through 21 show the present distribution of model hydrocarbons in the GRI corridor section. All figures plot the 100 and 200°C isotherms. It can be seen from Figures 12, for example, that the Jurassic source strata in the northern end of the Corridor are at present over 200°C (the dry gas window), while in the south these strata are ~150°C. As a result, the Jurassic source has produced more gas in the north than in the south.

Figure 12 shows the gas-oil mass ratio of migrating hydrocarbons at the present day, calculated for a migration pore fraction, S_{migr} , of 0.05%. The mass gas-oil ratio just above the Jurassic source strata is extremely high ($>10^5$). This ratio drops in a regular fashion to the south, reaching 0.8 just above the Jurassic source beneath the Jolliet reservoirs. When the Jurassic maturation products cross the Eocene source strata in the other half of the section, mixing with Eocene maturation products causes the GOR to drop. Below Tiger Shoals the GOR drops from 100,000 (the cutoff value) to 35 kg gas per kg oil, for example. The GOR decreases upward, but in the north remains quite high even at shallow depths. For example, the mass gas-oil ratio in the Tiger Shoals area at the present day ranges from 2.2 to 4.7. Thus hydrocarbons reaching the level of the Tiger

Shoals reservoirs (presently 2.6 to 5.5 km depth) are gas-rich enough to wash oils, perhaps to the extent observed. In addition, the GOR decreases to the south in a fashion that is compatible with the decrease in the intensity of gas washing to the south.

The mass fraction of hydrocarbons which is Jurassic CH_4 is shown in Figure 13. Between the Jurassic and Eocene source strata the migrating hydrocarbons are almost 100% gas. Seventy percent is methane and 30% CH_x . Even above the Eocene source, the fraction of Jurassic gas (methane plus wet gas) is over 50% of the total migrating gas everywhere, and over 80% of the gas almost everywhere (Figure 14).

Figure 15 shows, however, that Eocene oil is the dominant oil in strata overlying the Eocene source. This is because the Jurassic strata are in the dry gas window and are not generating Jurassic oil that could dilute the Eocene oils from below. Rather Eocene oils are mixing with previously-generated and migrated Jurassic oils in the higher parts of the section. This causes the mass fraction of Eocene hydrocarbon to decrease upward as shown in Figure 15.

Figures 12-15 in general show how earlier-generated, oil-rich hydrocarbon products are being flushed upward from the system by later-generated, more gas-rich hydrocarbons. The completeness of this flushing is of course dependent on the amount of hydrocarbon stored in the migration pathways compared to the amount generated in the source beds. This relationship is explored in Figures 16-20.

Figures 16 and 17 show how the present GOR of the migrating hydrocarbons would change if S_{migr} were decreased to 0.025% or increased to 0.1%. Figures 18 and 19 show how the Eocene fraction of total oil would change with these changes in S_{migr} . The distribution of oleanane and sulfur in the oils shown in Figure 9 would be very well matched by the fraction of Eocene oil shown in Figure 18. A comparison of Figure 16 with Figure 12 shows that there would also be more gas available in the northern part of the section to extensively wash the Tiger Shoals and SMI 9 oils as observed. For $S_{\text{migr}}=0.1\%$, Figures 17 and 19 show that there would be neither enough gas (relative to oil), nor enough Eocene oil relative to Jurassic oil in the upper part of the northern part of the section to account for the chemistry of the oils. The chemistry of the oils in the GRI corridor require that the migration mass fraction, S_{migr} , lie between 0.025 and 0.05%, and probably closer to 0.025%. Only if hydrocarbon retention during migration is this small can late-generated Eocene oils replace the earlier Jurassic oils as observed. Only if retention is low can late-generated Jurassic gas wash the Eocene oils as observed.

The migration fraction is low but not so surprisingly low as at first might be thought. Figure 17 shows that if the migration pore saturation, S_{migr} , is increased to just 0.5%, there is presently no venting of hydrocarbons from the model section, and that the reservoirs of all the study sites would be filled almost entirely with Jurassic oil. We know venting is occurring along the section, and the reservoirs in the north are filled with almost pure Eocene oil, so $S_{\text{migr}} = 0.5\%$ is an absolute maximum. In fact, to properly displace the Jurassic oils and provide a high enough GOR, S_{migr} must be much lower, $\sim 0.025\%$.

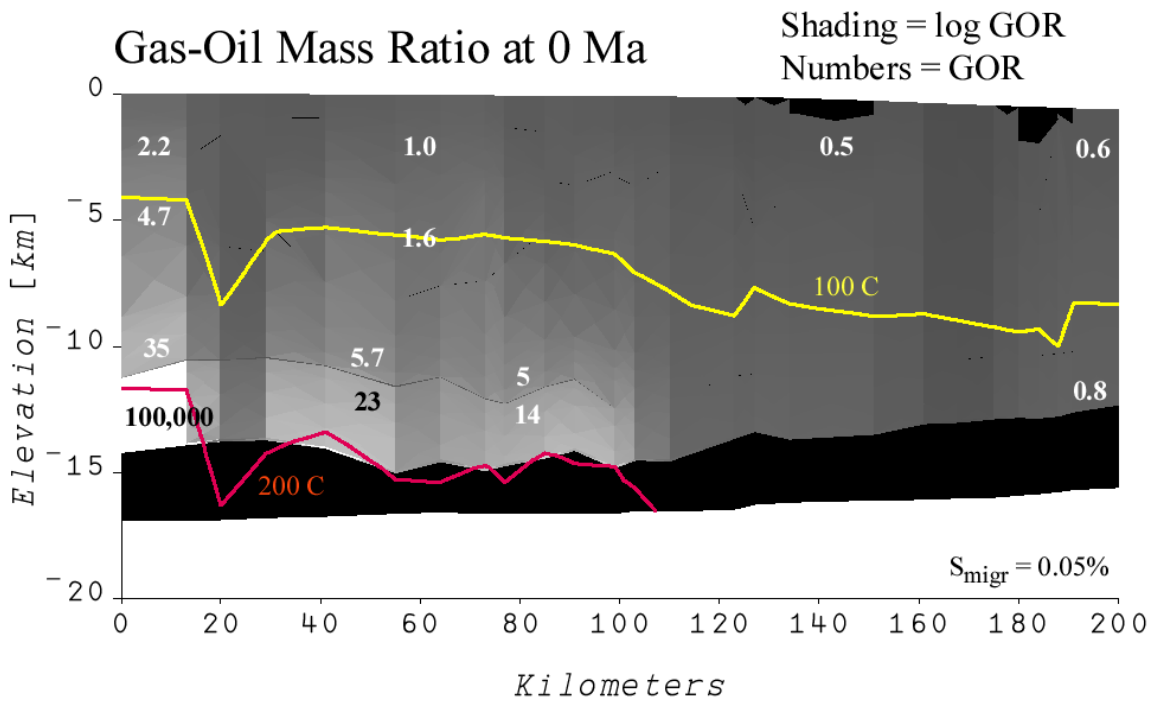


Figure 12. Gas-oil mass ratio in the section shown in Figures 6 and 7 for $S_{migr} = 0.05\%$.

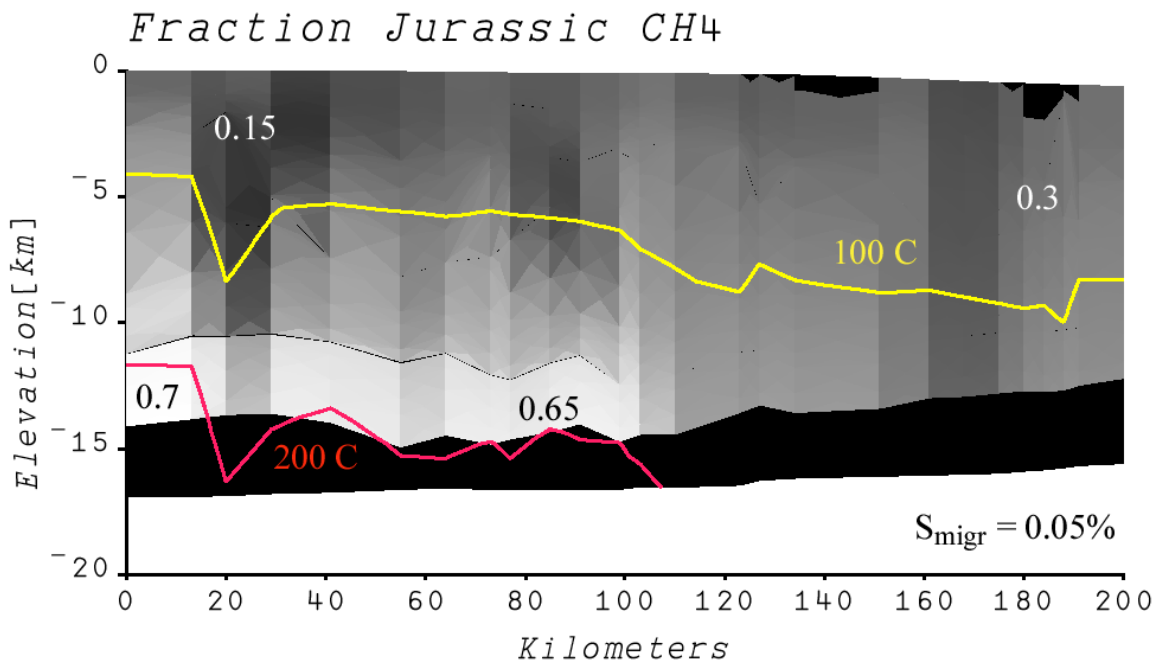


Figure 13. Mass fraction of Jurassic-sourced methane.

Fraction Eocene Gas of Total Gas

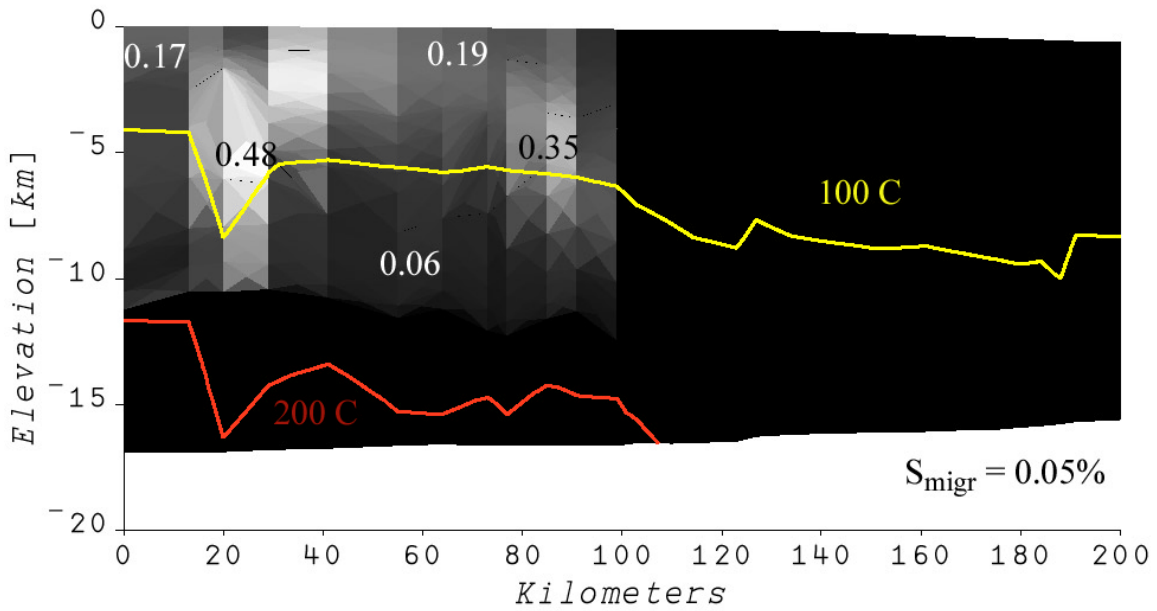


Figure 14. Eocene gas and condensate as mass fraction of the total gas and condensate.

Fraction Eocene Oil of Total Oil

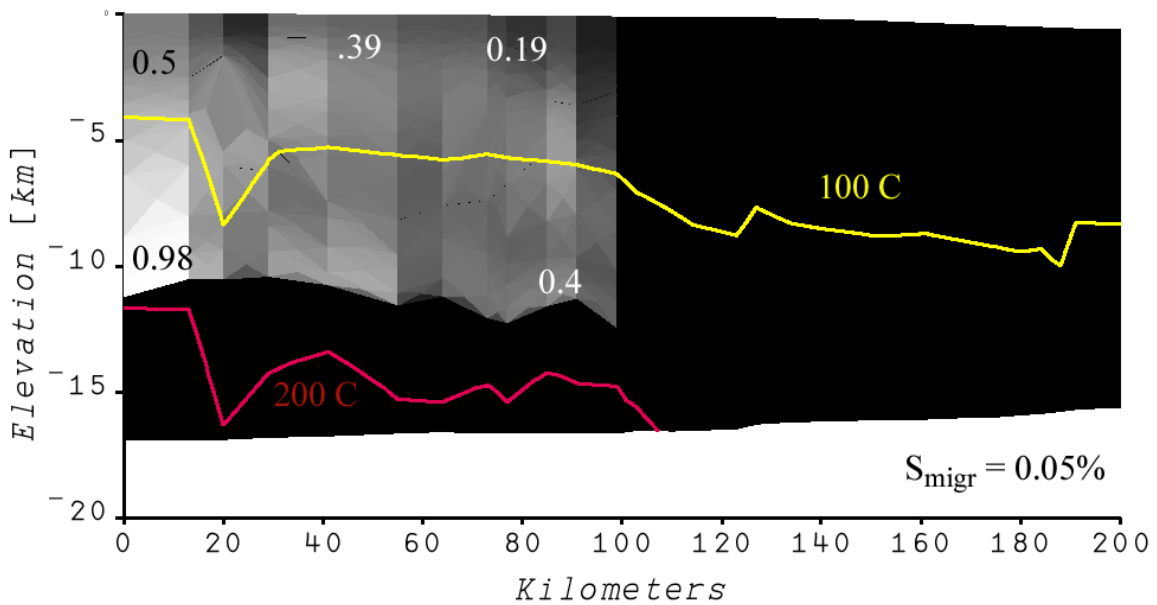


Figure 15. Fraction Eocene oil as a mass fraction of total oil.

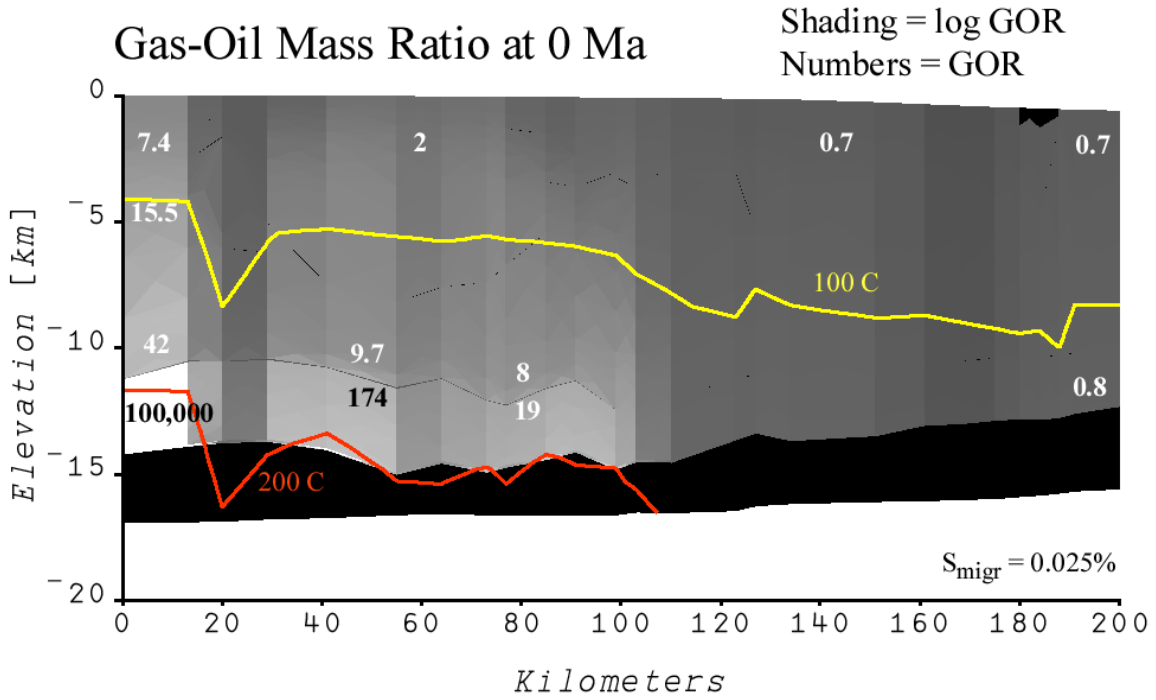


Figure 16. Gas-oil mass ratio in the section shown in Figures 6 and 7 for $S_{migr} = 0.025\%$.

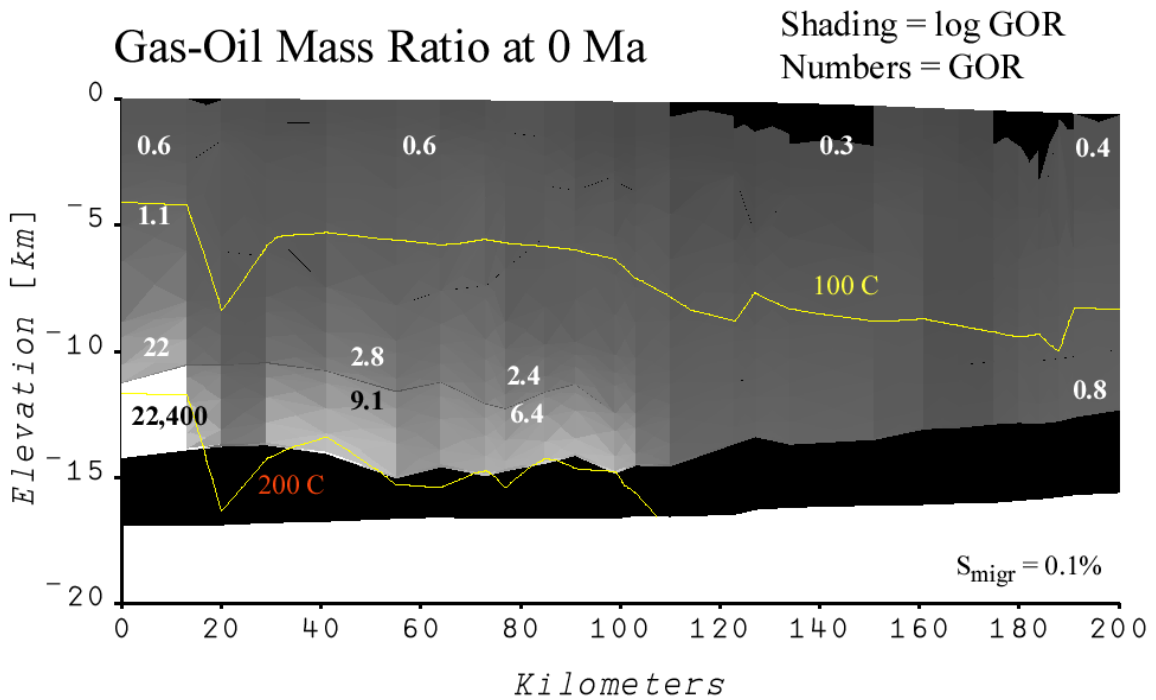


Figure 17. Gas-oil mass ratio in the section shown in Figures 6 and 7 for $S_{migr} = 0.1\%$.

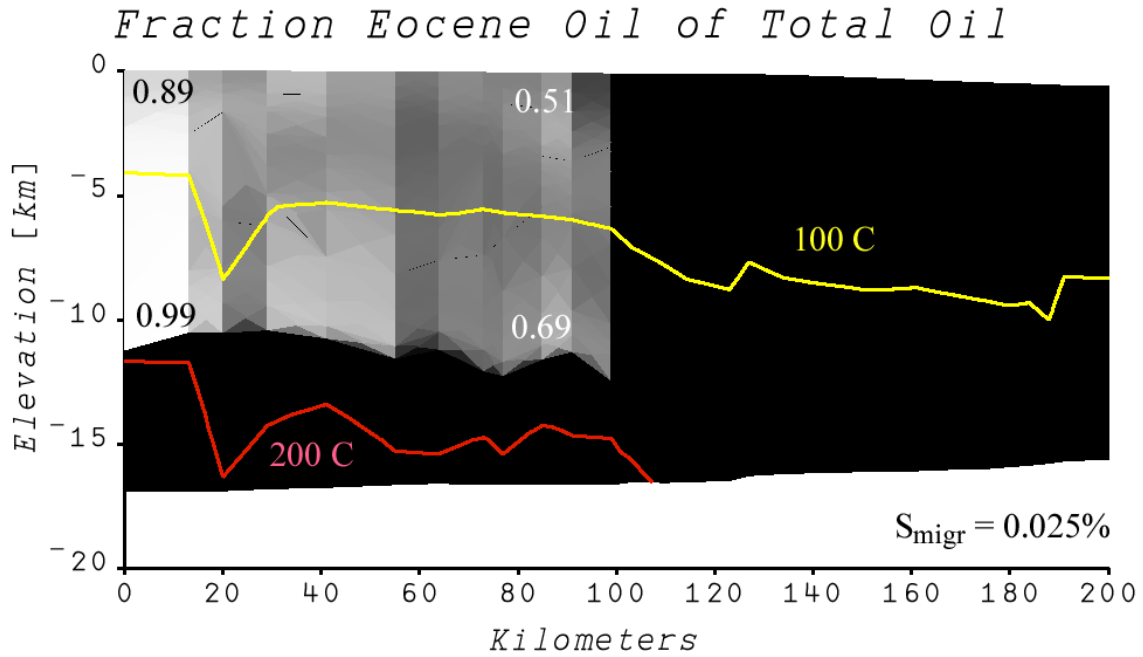


Figure 18. Eocene oil as mass fraction of the total oil in the section shown in Figures 6 and 7 for $S_{migr} = 0.025\%$.

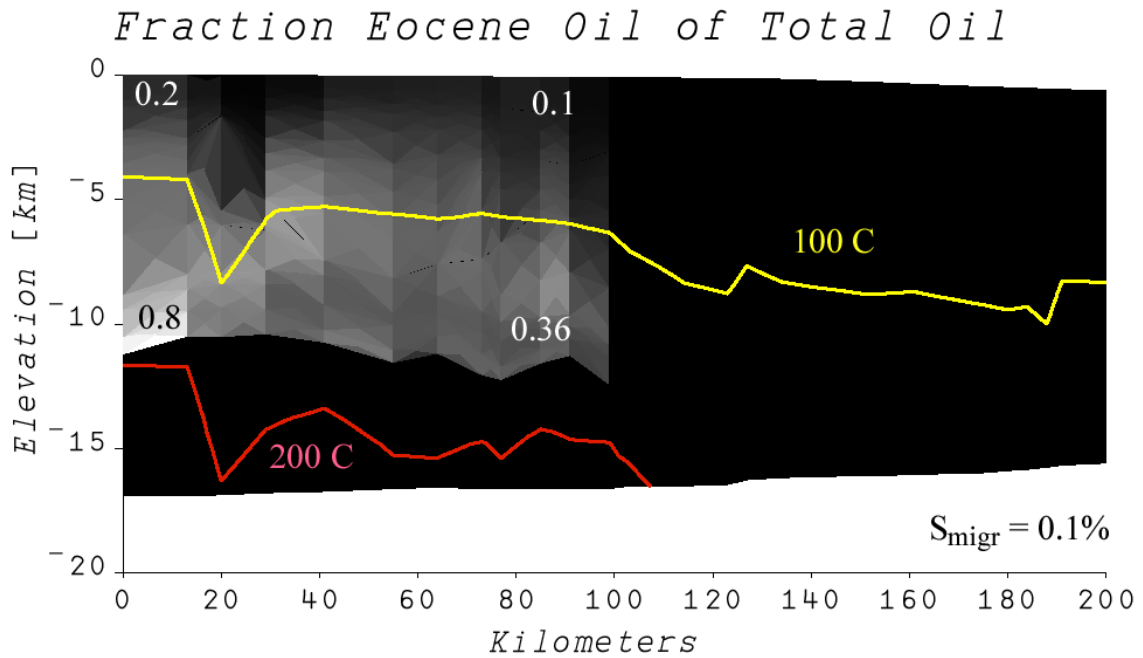


Figure 19. Eocene oil as mass fraction of the total oil in the section shown in Figures 6 and 7 for $S_{migr} = 0.1\%$.

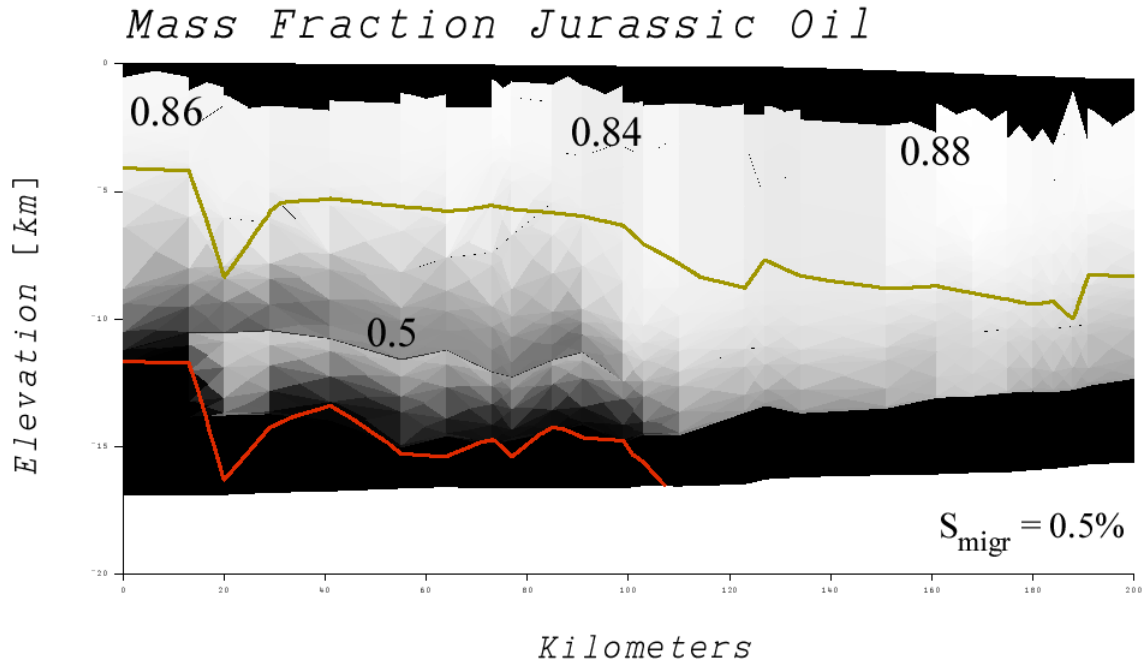


Figure 20. Mass fraction of Jurassic uncokable oil in the section shown in Figures 6 and 7 for $S_{migr} = 0.5\%$. For this migration fraction, no hydrocarbons are venting the surface at the present day.

An $S_{migr} \sim 0.025\%$ means that the hydrocarbon system in the GRI Corridor is a flow-through system in which there is very little retention of hydrocarbons in the migration pathways, and that massive amounts of hydrocarbon must have been vented into the Gulf as suggested in Figures 10 and 11 and Table 9. The retained hydrocarbons are replaced and altered as generation within the basin (by kerogen or hydrocarbon breakdown) continues.

f. Reservoir Filling and Washing at the 4 Corridor Sites

Details of the evolution of a hydrocarbon system can be best appreciated by considering processes occurring at specific sites within the Corridor. This approach allows us to assess the conditions under which the maturation rate of source strata in our model is sufficient to deliver hydrocarbons to the 4 Corridor sites in the recent time intervals that are geologically required, and to further probe the conditions under which oils in the north can be washed by gas to the degree observed. The situation at each site is slightly different, and we consider each in turn below.

1) Tiger Shoals

As summarized in Table 7, the reservoirs that constitute the Tiger Shoals field contain 0.133 Bbls oil, 0.43 Bbls condensate, and 6.4 TCF of gas in a 15×30 km area. The total hydrocarbon content of the area is 0.15 Bt with reservoirs hosting 0.0174 Bt oil, 0.0006 Bt condensate, and 0.129 Bt gas. The reservoirs are hosted in strata less than 16.5 Myrs old. The hydrocarbons have not been biodegraded, which requires that the oil reservoirs

(the shallowest is presently at 2.6 km depth) were filled when they were deep enough to have temperatures greater than $\sim 65^{\circ}\text{C}$ (see discussion in Volume IV of this series).

Figure 21 shows the mass flux and cumulative mass flux of hydrocarbons across the bottom half of the 10.1-8.8 Ma stratigraphic interval at -3.5 km below sea level depth at the location of Tiger Shoals. Hydrocarbon fluxes are computed assuming that a 20 vol% hydrocarbon saturation of the pore space is required for expulsion from the source beds, and that an 0.05 vol% saturation is required for hydrocarbon migration, as described above. Hydrocarbon flux across the 10.1 Ma time-stratigraphic horizon begins with its deposition. The upper half of the 10.1-8.8 Ma stratigraphic interval reaches 65°C about 5 Ma before present. From Figure 21 it can be seen that the average gas mass flux over the last 5 Myrs has been $\sim 3.5 \times 10^{-5}$ Bt/ km^2 -Ma. Assuming the reservoirs filled at this rate over a period of 1 Myrs, the radius from which hydrocarbons must be drawn to fill the reservoirs is 19.3 km, as shown in Figure 11. This is reasonable. It is a dimension similar to that of the 15×30 km area that contains the reservoirs.

Figure 22 shows that the 0.0174 Bt of oil can be provided in 1 Myr at the present oil migration rate for a similar draw radius of 13.2 km. The 0.0174 Bt of oil can be washed in 1 Myr with a mass GOR ratio >3.5 for a draw radius of 13.3 km. Figure 23 shows that the oil will be over half Eocene-sourced oil if the reservoirs are filled after ~ 5 Ma. Furthermore, the mass gas-oil ratio increases strongly with time. Thus oil in the migration pathway can be washed with gas dryer than that from which it fractionated. Figure 24 shows how the mass gas-oil ratio and mass fraction of Eocene to total oil depends on the migration fraction, S_{migr} , and time. For $S_{\text{migr}} \sim 0.025\%$, the GOR is high enough to allow gas washing, and the fraction Eocene oil is high enough for the oil chemistry to match the observed composition (Figure 9).

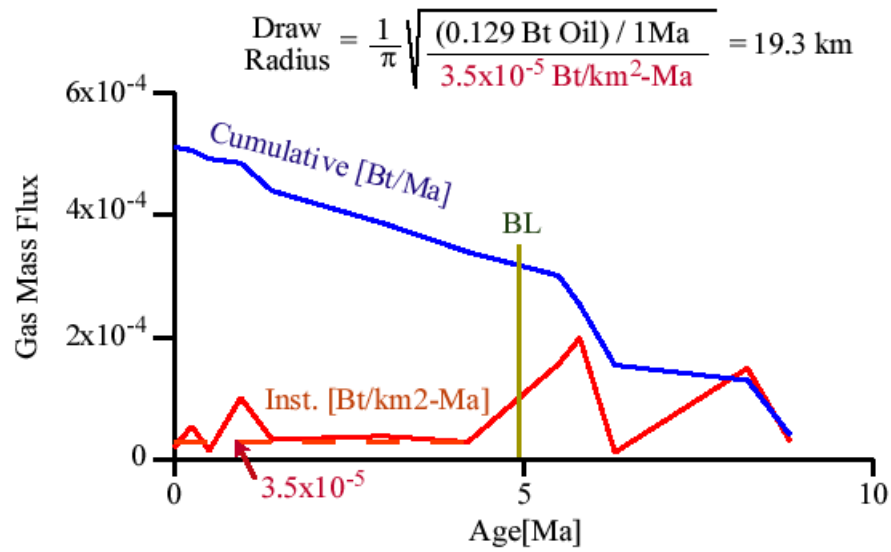


Figure 21. The cumulative and instantaneous mass flux of gas across the 10.1 Ma time-stratigraphic horizon at Tiger Shoals (see Figure 6 for location). BL is the biodegradation limit, which is the time at which the upper half of the 10.1 to 8.8 Ma stratigraphic interval reached 65°C. A draw radius of 19.3 km will capture enough gas in 1 Myr to fill the 0.129 Bt of gas in the Tiger Shoals Reservoirs. The reservoirs could have filled in any 1 Myr interval over the last ~5 Myrs.

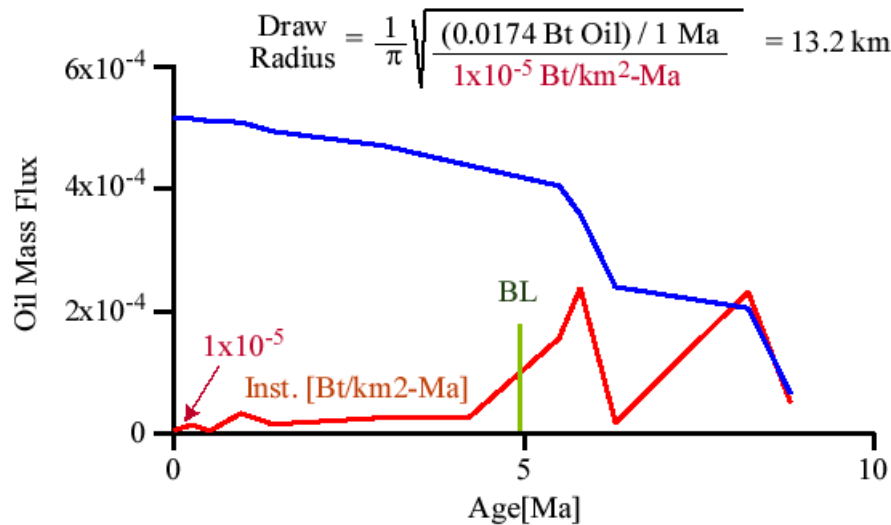


Figure 22. The cumulative and instantaneous oil mass flux of oil across the 10.1 Ma time-stratigraphic horizon at Tiger Shoals (see Figure 6 for location). BL is the biodegradation limit (the time at which the upper half of the 10.1-8.8 Ma stratigraphic interval reached 65°C). At the present oil migration rate, a draw radius of 13.2 km will capture enough oil over a 1 Ma period to introduce 0.0174 Bt of oil into the Tiger Shoals Reservoirs. Oil could be introduced much faster at times closer to 5 Ma. The oils in the reservoir could be washed with a GOR of 3.5 by the current stream of migrating gas in 1 Ma and a draw radius of 13.3 km.

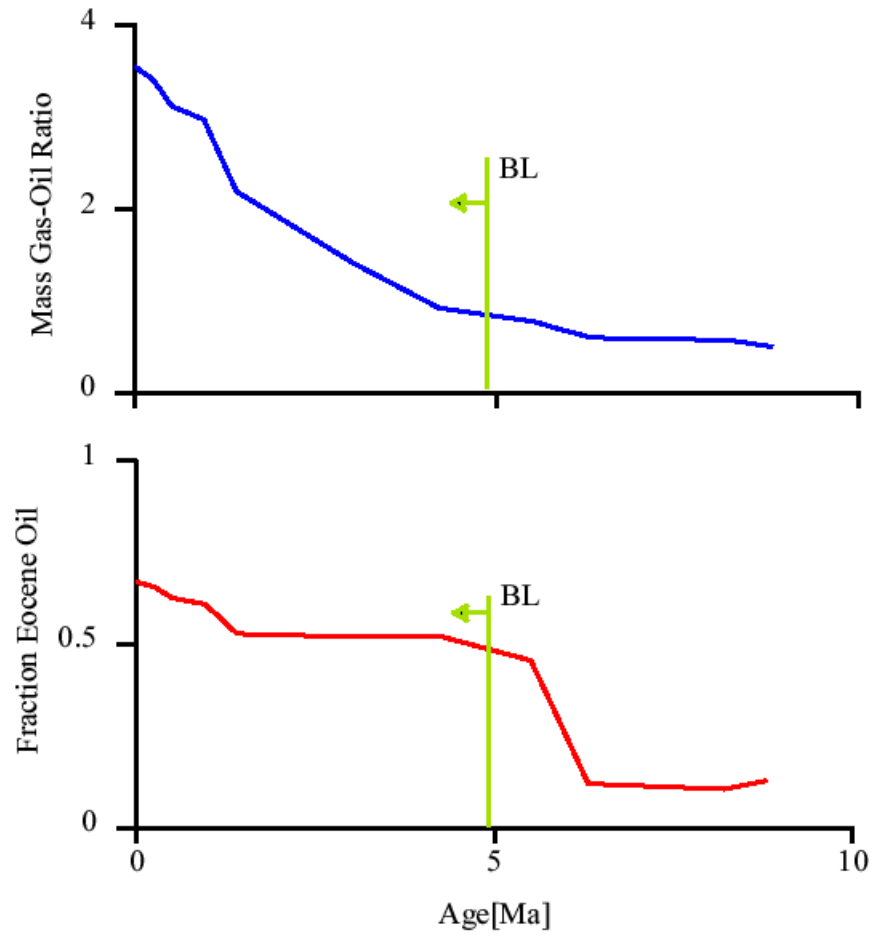


Figure 23. (a) The mass gas-oil ratio of the hydrocarbons filling the Tiger Shoals reservoirs as a function of time. (b) The fraction Eocene sourced maturation products passing the 10.1 Ma time-stratigraphic horizon at the Tiger Shoals location as a function of time. BL is the biodegradation limit from Figure 21 and 22.

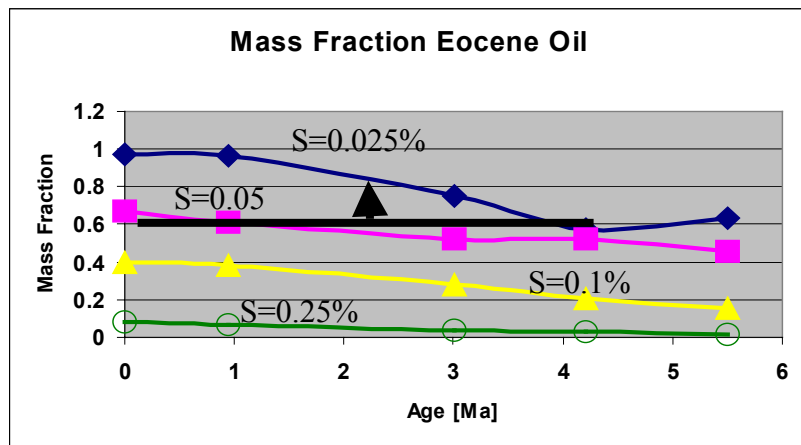
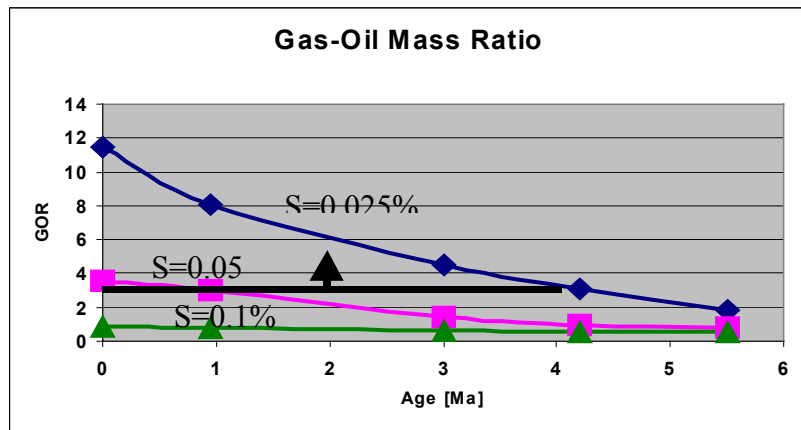
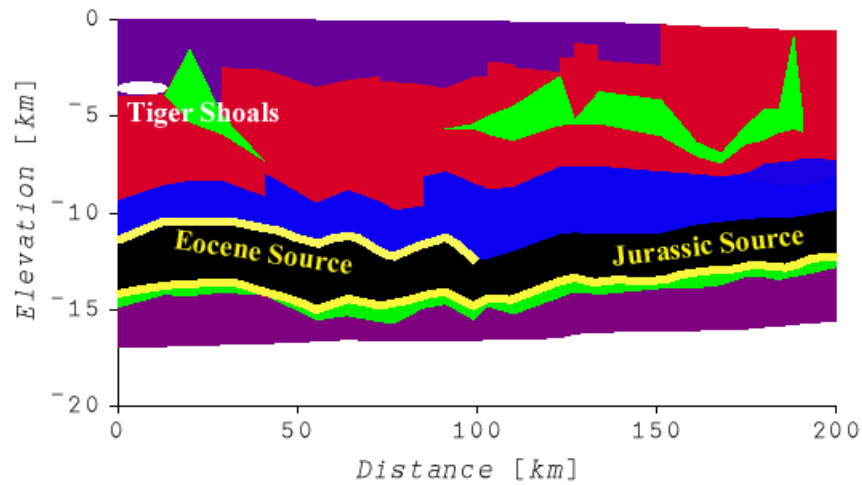


Figure 24. (a) GRI Corridor showing the location of the 10.1 Ma horizon in the Tiger Shoals Reservoirs (the oval labeled Tiger Shoals) and the Eocene and Jurassic source strata. (b) Model gas-oil ratio by weight of hydrocarbons at the Tiger Shoals location in (a) as a function of the migration fraction and time. A GOR of 3.5 is assumed in the draw radius calculations (bar with vertical arrow). (c) The mass fraction of Eocene oil as a function of S_{migr} and time at the location shown in (a). The mass fraction of Eocene oil must be greater than ~ 0.6 (bar with vertical arrows).

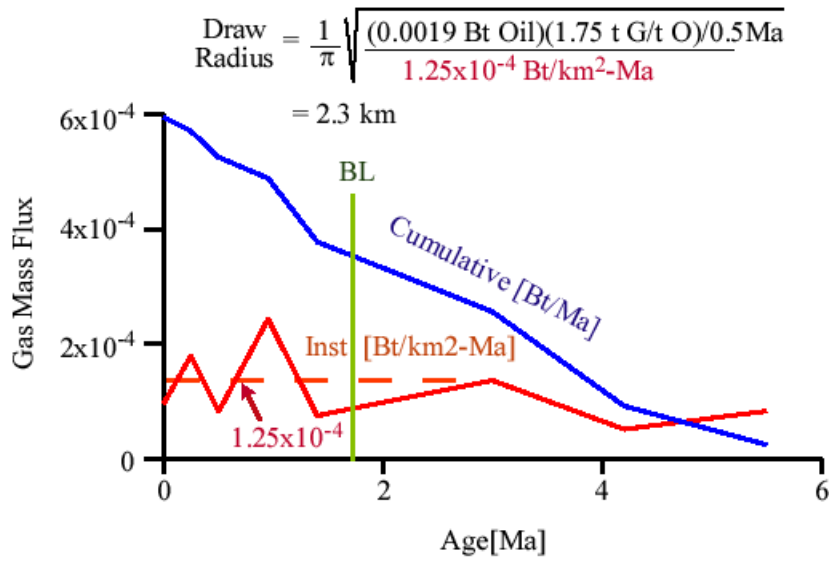


Figure 25. The cumulative and instantaneous mass flux across the 5.8 Ma time-stratigraphic horizon in the SMI 9 area located in Figure 6. BL is the biodegradation limit (the time at which the upper half of the stratigraphic interval between 5.8 and 8.2 Ma reaches 65°C). The draw radius will capture enough gas over 0.5 Ma to wash the 0.0019 Bt of oil in the South Marsh Island Block 9 Reservoirs at a gas-oil mass ratio of 1.75.

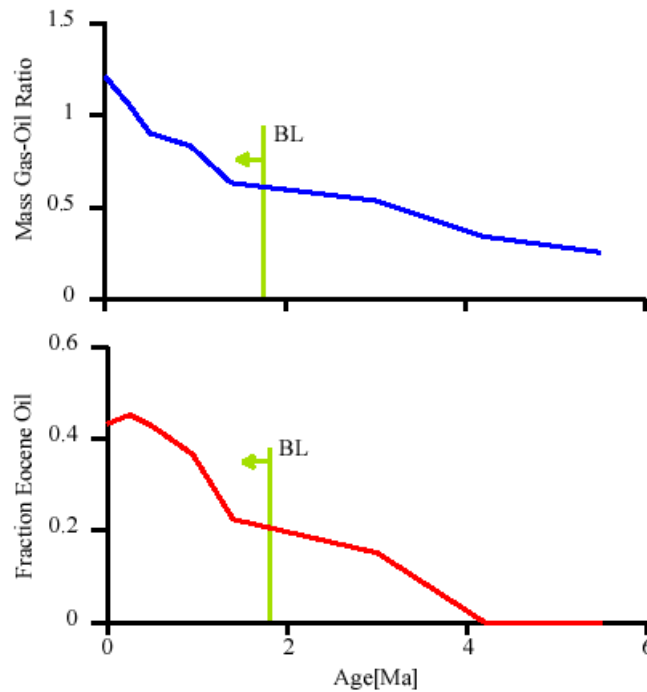


Figure 26. (a) The mass gas-oil ratio of the hydrocarbons filling the South Marsh Island 9 reservoirs as a function of time. (b) The fraction of Eocene sourced maturation products passing the 5.8 Ma time-stratigraphic horizon at the South Marsh Island 9 location as a function of time. BL is the biodegradation limit from Figure 25.

$$\text{Draw Radius} = \frac{1}{\pi} \sqrt{\frac{(0.04 \text{ Bt Oil}) / 0.23 \text{ Ma}}{9.25 \times 10^{-5} \text{ Bt/km}^2 \cdot \text{Ma}}} = 13.8 \text{ km}$$

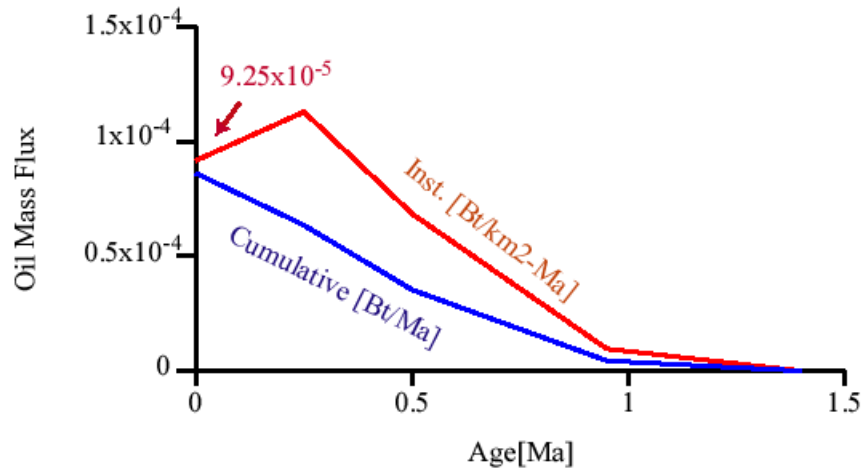


Figure 27. The cumulative and instantaneous mass flux across the 3 Ma time-stratigraphic horizon in the Eugene Island Block 330 area located in Figure 6. The reservoirs filled in the last 0.23 Ma. The draw radius will capture enough oil over 0.23 Ma to fill the Block 330 reservoirs.



Figure 28. The mass gas-oil ratio of the hydrocarbons filling the Eugene Island Block 330 reservoirs as a function of time. The reservoirs filled in the last 0.23 Ma.

$$\text{Draw Radius} = \frac{1}{\pi} \sqrt{\frac{(0.0044 \text{ Bt Oil}) / 0.02\text{Ma}}{1.52 \times 10^{-4} \text{ Bt/km}^2\text{-Ma}}} = 12.1 \text{ km}$$

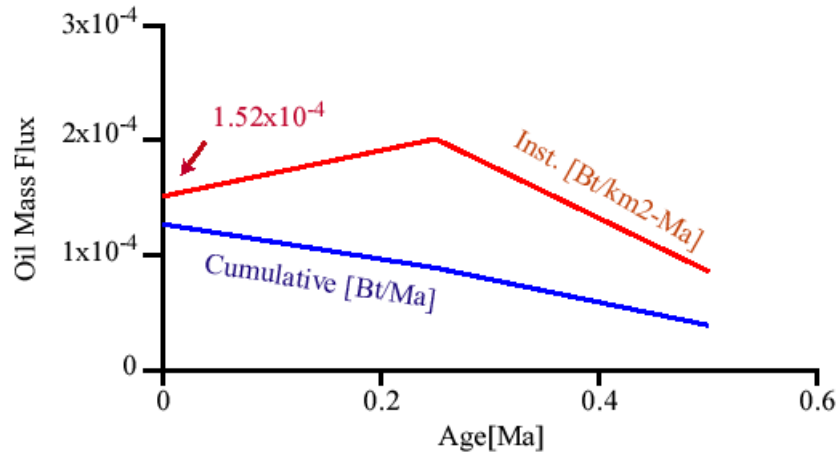


Figure 29. The cumulative and instantaneous oil mass flux across the 0.95 Ma time-stratigraphic horizon in the Jolliet area located in Figure 6. The Jolliet reservoirs filled in the last ~20,000 years. A draw radius of 12 km will capture enough oil to fill the reservoirs in 0.02 Ma..

$$\text{Draw Radius} = \frac{1}{\pi} \sqrt{\frac{(0.0031 \text{ Bt Gas}) / 0.02\text{Ma}}{8.48 \times 10^{-5} \text{ Bt/km}^2\text{-Ma}}} = 13.6 \text{ km}$$

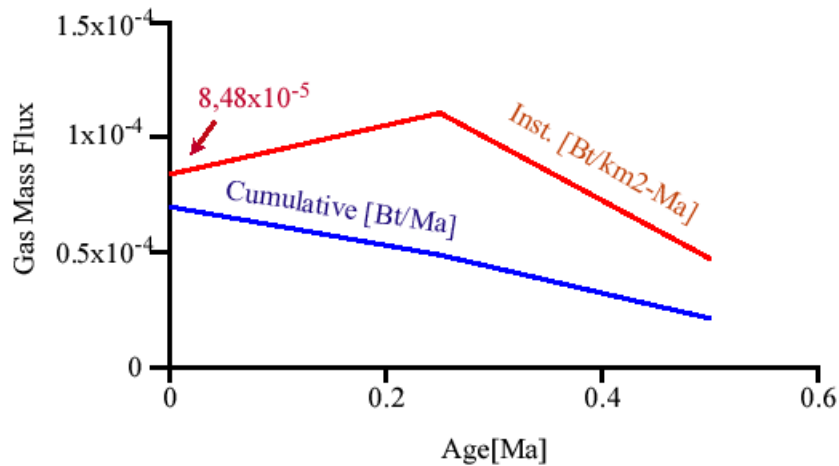


Figure 30. The cumulative and instantaneous gas mass flux across the 0.95 Ma time-stratigraphic horizon in the Jolliet area located in Figure 6. The Jolliet reservoirs filled in the last ~20,000 years. A draw radius of ~14 km will capture enough gas to fill the reservoirs in 0.02 Ma. The gas discharge rate from the Jolliet system at present is ~49 t/a. The mass gas-oil ratio of the discharge is 0.55.

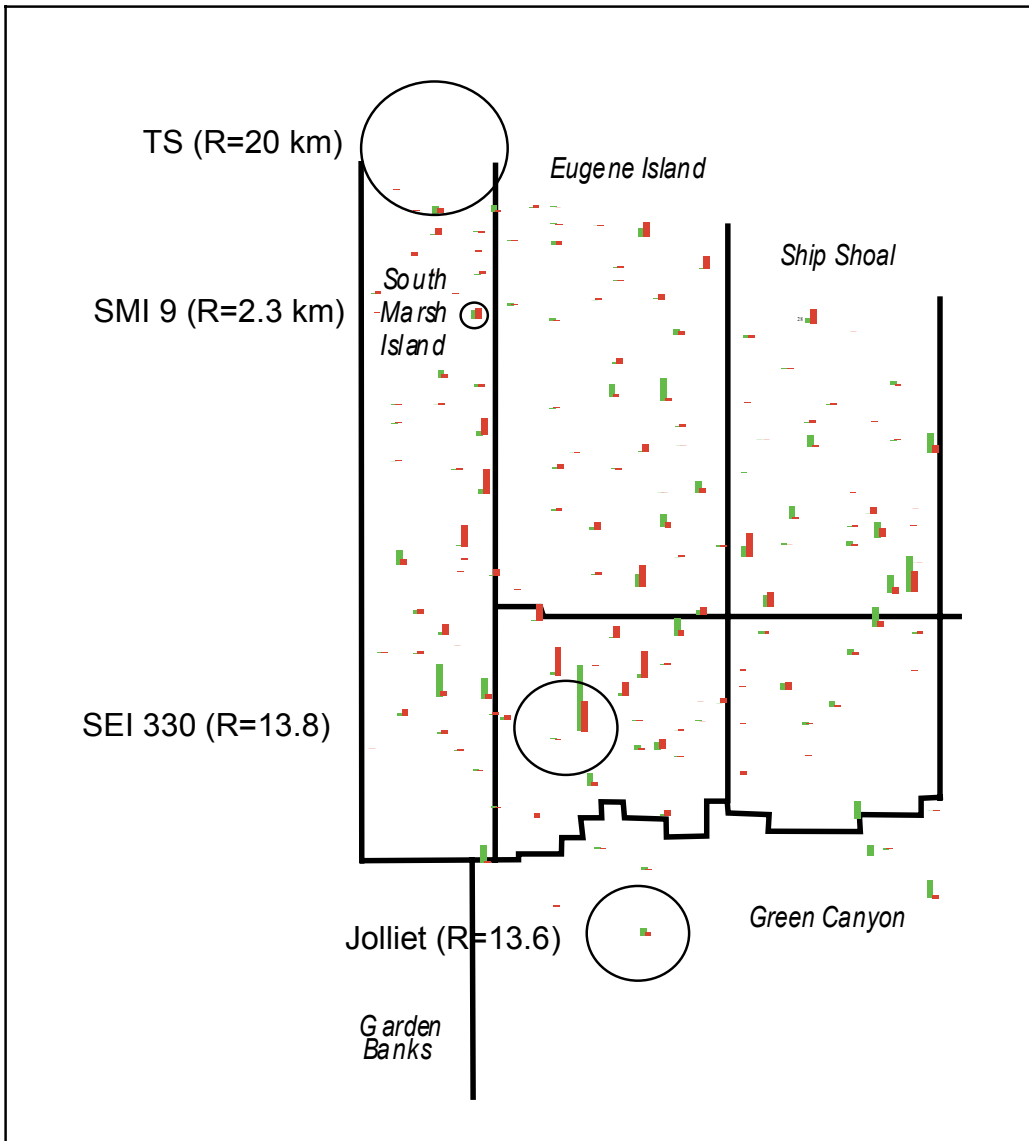


Figure 31. Draw areas from Figures 21, 25, 27, and 30 are plotted against hydrocarbon resource histograms (oil green, gas red) from Bascle et. al. (1999).

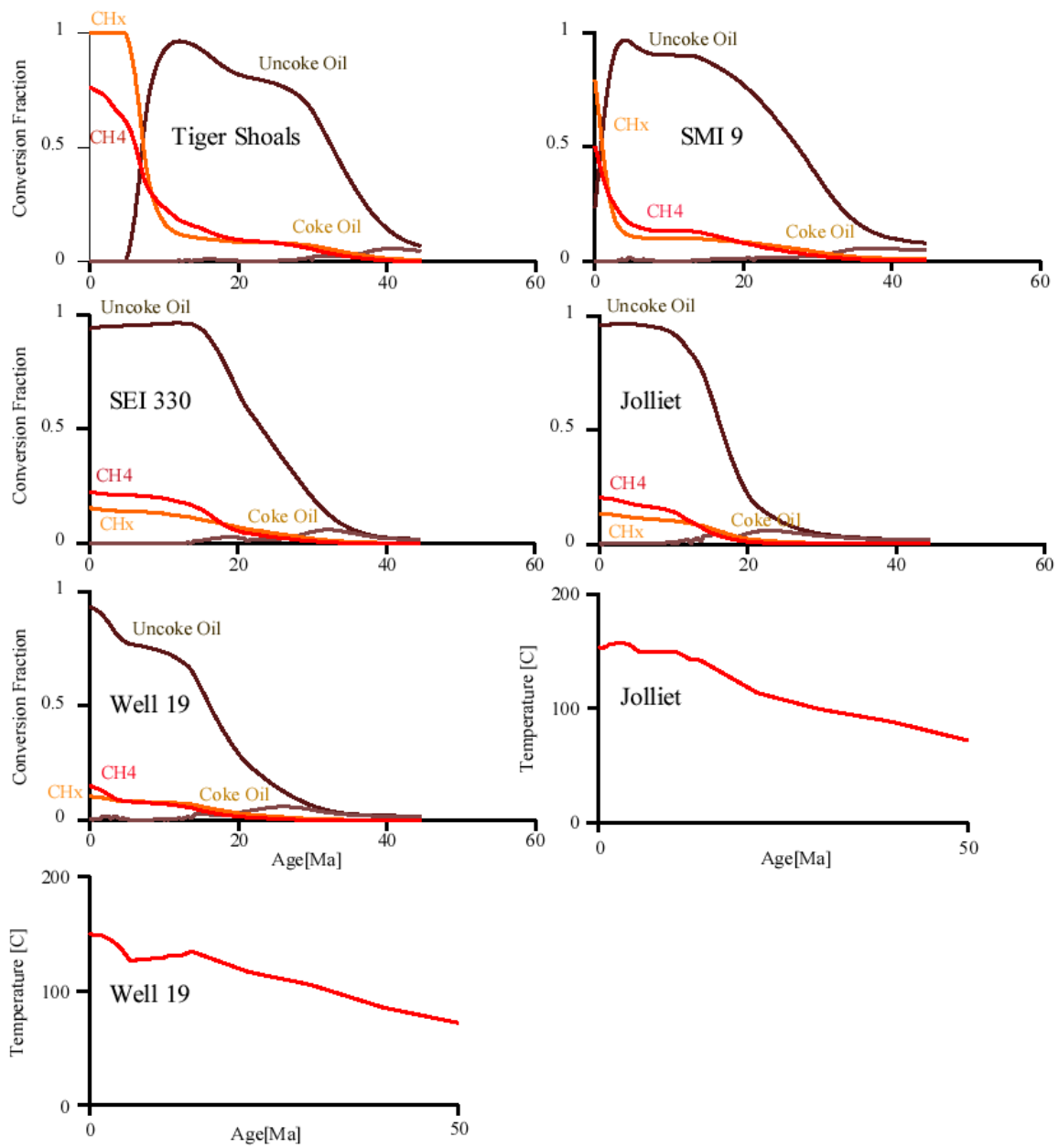


Figure 32. Conversion fractions and temperatures in the Jurassic source bed under Tiger Shoals, SMI9, SEI 330, Well 19 (between SEI330 and Jolliet 164 km across section), and Jolliet. Fractional conversions are calculated assuming all hydrocarbon maturation products remain in the source strata (e.g., that there is no hydrocarbon migration).

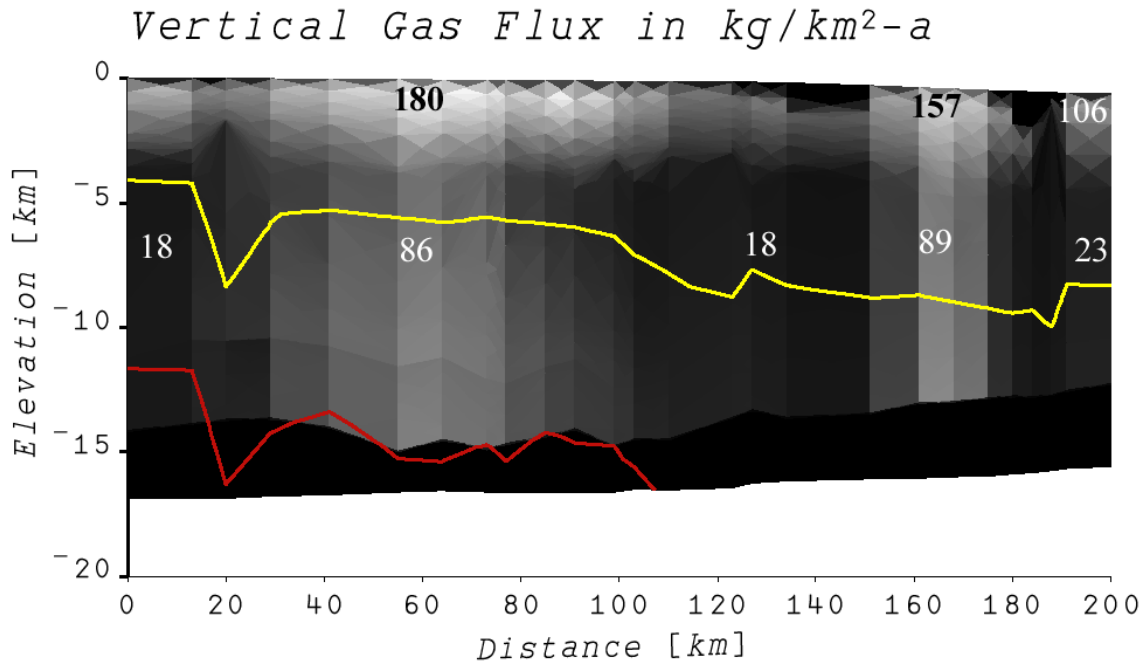


Figure 33. Vertical gas mass flux in $\text{kg}/\text{km}^2\text{-a}$. The increase in mass flux above ~ 3 km depth is caused mainly by compaction. The gas mass flux at Jolliet (2 km depth) is $70 \text{ kg}/\text{km}^2\text{-a}$. The mass flux at well 19 is between 89 and $157 \text{ kg}/\text{km}^2\text{-a}$. At 2 km depth the gas flux in well 19 is $138 \text{ kg}/\text{km}^2\text{-a}$. The cause of the increased venting in well 19 is a rapid increase in temperature over the last ~ 3 Ma caused by sedimentation and salt diapirism.

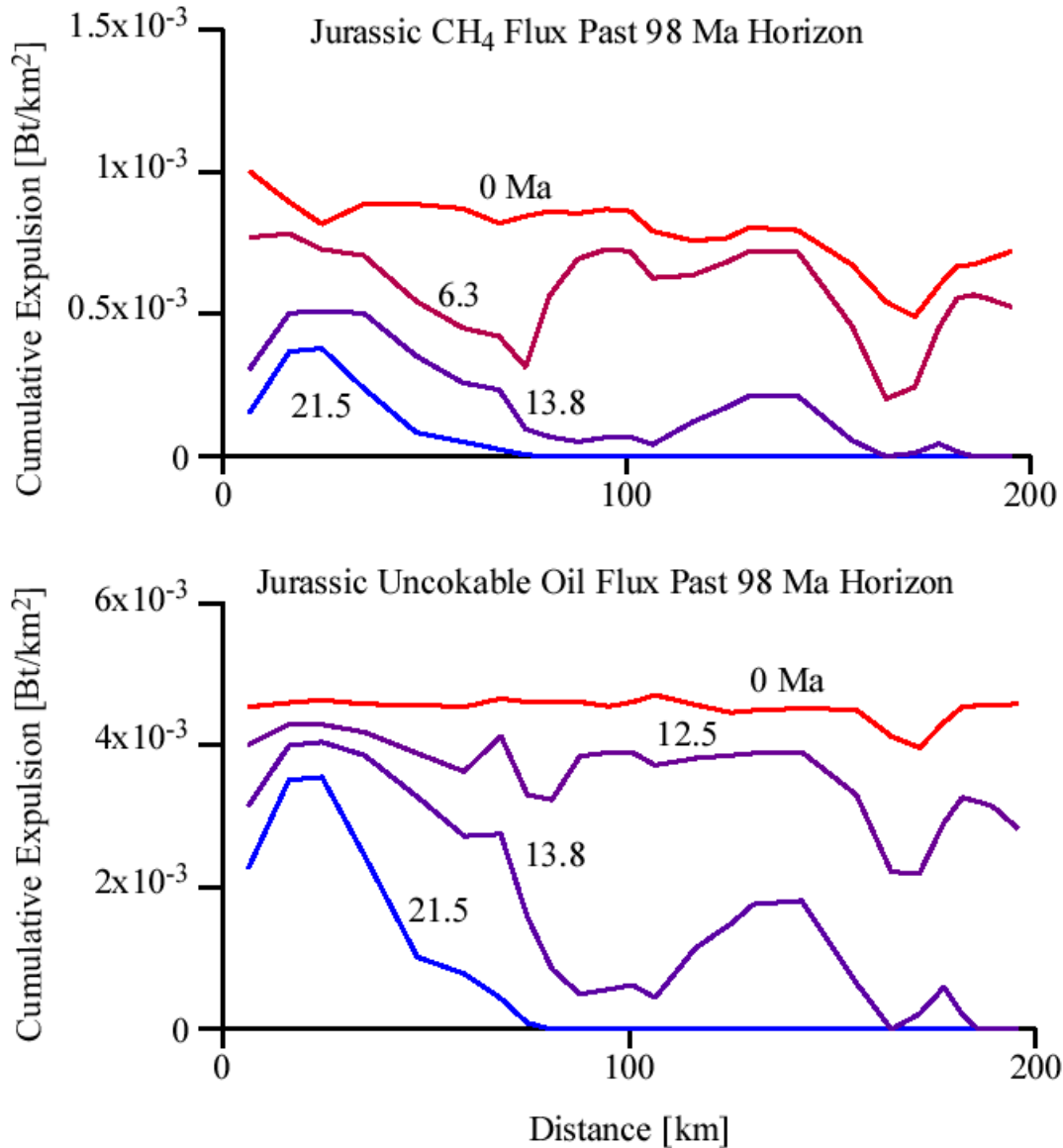


Figure 34. (a) Upper diagram: cumulative mass flux of Jurassic-sourced methane and uncokable oil through the 98 Ma horizon as a function of time. (b) Lower diagram: cumulative vertical hydrocarbon flux across the 9.8 Ma horizon from north to south with time across the 200 km GRI Corridor.

2) South Marsh Island 9

The South Marsh Island Block 9 area hosts 0.0046 Bt of hydrocarbons in strata 2.6 to 5.7 km below the sea floor (see Table 9). The SMI 9 oils are not biodegraded. Figure 25 examines the mass fluxes across our model 5.8 Ma horizon lying presently ~3.4 km below the sea level. This horizon exceeded 65°C at about 1.8 Ma. The gas mass flux has been ~1.25 x 10⁻⁴ Bt/km²-Ma since 1.8 Ma. The 0.0019 Bt of oil in the SMI 9 reservoirs can be washed at a mass gas-oil ratio of 1.75 in 0.5 Ma if hydrocarbons are drawn from a radius of 2.3 km.

Figure 26 shows that the oils will be mostly from the Eocene source after ~1.5 Ma. Figure 9 suggests some of the oil is Jurassic at the SMI 9 location. The GOR is increasing and thus dryer gas is available for washing. The GOR would be above 2 for $S_{migr} = 0.025\%$ (see Figure 16).

3) Eugene Island Block 330

The South Eugene Island Block 330 area hosts 0.04 Bt of oil and 0.03 Bt of gas in strata 1.4 to 2.4 km below the sea floor in 0.9 to 1.75 Ma strata (see Table 9). Figure 27 shows that the flux of oil across the 3.0 Ma model horizon ~2.3 km below present sea level is sufficient to fill the oil reservoirs in 0.23 Ma if hydrocarbons are drawn from ~14 km. Geologic evidence suggests the reservoirs have been filled in the last 0.09 to 0.23 Ma (Table 9). Figure 28 shows that the GOR of hydrocarbons passing the 3 Ma horizon during filling is ~0.55. Only the deepest (OI sand) oils are washed, and these are washed only slightly (15% mass depletion of n-alkanes).

4) Jolliet

The Jolliet area hosts 0.0044 Bt of oil and 0.031 Bt gas in 0.6 to 1.8 Ma strata lying 1.2 to 2.4 km below the sea floor (see Table 9). Figure 29 shows that the mass flux of oil across our model 0.95 Ma horizon ~2 km below present sea level is sufficient to fill the reservoirs in 20,000 years if the oil is drawn from distances of ~12 km. Figure 30 shows that the gas reservoirs can be filled if gas is drawn from ~14 km. With this draw, the model gas venting rate is 49 tonnes per year.

5) Corridor Characteristics

Figure 31 plots the draw radii for the 4 GRI study sites discussed above against a background of hydrocarbon resource (produced plus discovered reserved) histograms. The draw radii are reasonable for these four sites in the sense that the calculated draws allow hydrocarbons to be drawn to the study sites without obvious conflict with neighbor sites of discovered resources.

The rate of hydrocarbon expulsion from source strata is controlled by the stage of maturation as well as the heating (sedimentation) rate. All things equal, expulsion will be greater in the gas stage because gas is less dense than oil. When all phases in the source strata have reacted as fully as possible, expulsion will cease. Figure 32 plots conversion fractions for hydrocarbons in the Jurassic source under the 4 sites discussed above, assuming (for illustration) there is no migration from the source strata. Differences in the stage of maturation across the section are apparent. In the north (Tiger Shoals), uncokeable oil in the source has been fully cracked to methane. Production of CH_x has ceased, but CH_4 continues to be produced, at a slower rate, from the breakdown of char (see Table 4). At South Marsh Island Block 9, oil cracking is occurring at close to its maximum rate, producing both CH_x and CH_4 . Driven by this gas, migration of both oil and gas is particularly rapid in this area. Temperatures in the Jurassic source beneath South Eugene Island Block 330 and Jolliet are high enough that oil production has ceased, but not high enough to cause any significant cracking of oil to gas.

The pattern of vertical gas flux along the GRI Corridor is depicted in Figure 33. The relative maximum at SMI 9 60 km across the section is evident, as well as a maximum ~164 km across the section. There is also an increase in mass flux in the upper ~3 km of the section.

The increase in mass flux above about 3 km depth is a possibly-realistic artifact of compaction and our migration rules. The migration rule we use is that hydrocarbons move vertically to the next element when the fraction of hydrocarbons in the pore space exceeds S_{migr} . Therefore if hydrocarbons are venting to the surface, as here, compaction of the sediments will squeeze hydrocarbons from the pore space, and increase the hydrocarbon migration flux by ~2 or more. This may be realistic because hydrocarbons may pond and spill in the relatively dynamic shallow subsurface.

The increase in vertical mass flux at ~60 km is due to the rapid conversion there of oil to gas in the Jurassic source strata. The increase in mass flux at 164 km is due to a comparatively rapid deposition of sediments in that area. This location is the axis of the second salt-withdrawal minibasin, and has received the most sediments since filling started at 5.8 Ma (see Figure 7).

Finally Figure 34 shows the cumulative flux of Jurassic-sourced methane and uncokeable oil past the 98 Ma horizon. This figure shows how gas and oil generation has shifted with time from northern to the southern parts of the GRI Corridor.

E. Summary, Discussion, and Future Work

1. Summary

We have constructed a physical model of a 125×200 km portion of the offshore Louisiana Gulf of Mexico Basin from basic first principles. We start by inferring crustal extension from sediment thickness and water depth along a 1050 km long section that extends from the Arkansas-Louisiana border to the Sigsbee Knolls. A 150 km thick plate rifting model is then used to determine the heat flow to the base of the sediment section. The plate model computes the thermal effects of extension and sediment deposition at the geologically observed rates, and takes into account radiogenic heat production in the crust and basin sediments. The heat flows to the base of the sediment section thus determined are then used in a basin model in which critical parameters such as thermal conductivity and radiogenic heating are carefully modeled as a function of compaction, temperature and lithology. The computed heat flows and subsurface temperature gradients reproduce both the unusually low surface heat flow (~half normal) and present temperature gradients along the 1050 km section remarkably well, especially considering no parameters were adjusted once selected from the literature.

The computed temperature history is then used to mature both Jurassic and Eocene source rocks in the 125 by 250 km GRI Corridor. The hydrocarbon system is abstracted from the literature and consists of an Eocene source bed 30 m thick underlying the northern half of the Corridor, and a Jurassic source bed under the entire Corridor (Table 8, Figure 24). The maturation models are standard (Tables 4 and 5). The model

hydrocarbons are migrated and mixed with one another assuming expulsion from source occurs at 20 vol% hydrocarbon saturation of the pore space, and that migration requires a ~0.05 vol% pore space saturation. To our knowledge this is the first modeling study that explicitly models the generation and mixing of hydrocarbons generated from two different sources whose maturation products can be chemically distinguished. Application of this model to the GRI Corridor, where we have carefully assembled diverse chemical data on the oils and gases, yields a surprisingly large number of important conclusions:

1. The source beds in the GRI Corridor have almost completely matured. As summarized in Table 9, vastly more hydrocarbons have been generated and expelled from the source strata (186 Bt) than have been discovered in producible reservoirs (1.35 Bt).
2. Gas and oil are venting from innumerable seeps in the Corridor. Our modeling indicates this could not occur unless the retention of hydrocarbons in pore space along the migration pathways connecting the source strata to the surface is less than 0.5% of that pore space (Figure 20).
3. Hydrocarbon chemistry requires that retention of hydrocarbons in migration pathways is 10 times less than this, or <0.05%. Only if this is the case can Eocene-sourced oils displace earlier-generated Jurassic-sourced oils in the northern half of the section as is required by field data (Figure 9). At the venting limit (0.5%), shallow oils are Jurassic (Figure 20), so the oils must have been displaced. For a migration fraction of 0.025%, the Jurassic oils are displaced such that the shallow oils at the north end of the Corridor are ~90% Eocene and half way across the section are ~50% Eocene. This change is similar to that suggested by sulfur and oleanane data (compare Figure 18 and 9).
4. Washing of Eocene oils in shallow migration pathways can be accomplished if they interact at shallow depths with Jurassic dry gas. Jurassic gas floods the section (Figure 14) and the gas-oil ratio is high enough to accomplish the washing (Figures 12, 16, 24, and also Figures 21-30).
5. The decrease in gas washing to the south parallels and is logically explained by the decrease in GOR (Figures 12 and 16).
6. All the reservoirs have filled recently. This is indicated by the lack of biodegradation of the oils in the northern half of the corridor (Tiger Shoals, SMI 9, ~SEI 330), and by geologic constraints in the southern half of the Corridor (SEI 330, Jolliet).
7. If hydrocarbons are drawn from distances of 2 to 20 km, the reservoirs in the 4 GRI study sites could be filled with hydrocarbons at the model migration rates in < 1 Ma, or in the much shorter time intervals required by geological constraints at the southern sites (Figures 21-30). The draw radii are of the same scale as salt withdrawal minibasins in the area.
8. The 2 to 20 km draw radii are reasonable in terms of the distribution of discovered hydrocarbon reservoirs (Figure 31).
9. The rate of gas venting inferred at Jolliet is supported by a recent independent estimate based on the mass of gas hydrate that has accumulated at a Jolliet surface vent (see discussion below).

10. With low retention along migration pathways, the amount of hydrocarbons vented into the ocean from the GRI Corridor is massive (131 Bt; Table 9). This is equivalent to over 1000 billion barrels of oil, or more hydrocarbon than has been produced and consumed by humans since the start of the petroleum era. At least in this area of the Gulf of Mexico Basin humans are, in effect, intercepting hydrocarbons from a massively leaky flow-through petroleum system that would otherwise vent naturally. If this is a general situation, human hydrocarbon usage may have less impact than otherwise might be imagined.
11. All the above suggests that the hydrocarbon reservoirs in the GRI Corridor are ponds along migration conduits that may persist for protracted periods of geologic time, but whose contained hydrocarbons are constantly replenished and replaced by the introduction of new hydrocarbons.
12. Hydrocarbon chemistry reflects current, large scale, and significant basin processes that can be unlocked by basin models that compute the generation and migration of hydrocarbons from two or more sources. Chemical variations interpreted by more refined models could have exploration utility (see below). Low migration retention allows new parameters such as draw radius to be calculated from basin models that could also have exploration utility.

2. Discussion

Although a significant advance, the Corridor models need to be further refined. Figure 32 shows, for example, that the location of minibasins with high sediment deposition rates can affect the rate of hydrocarbon generation by a factor of 2 or more. Our Corridor analysis is based on generalized geology from 50 km to the east. The general trends are reliable, but the minibasins and sediment history are not accurately tied to the geology along the section. We have also reduced the heat flow by 10% to increase the vigor of hydrocarbon maturation at the present day. This is a simple modeling way to decrease the depth of the Jurassic source, but means the near-surface temperature gradients in our model are lower than observed. This is not important to present conclusions, but would be important if biodegradation becomes a more critical aspect of the analysis.

The nature and general validity of the present results are illustrated by comparison to a recent independent determination of gas venting rates in the Jolliet system. Chen and Cathles (in press) estimate the rate of gas venting from the Jolliet system using a kinetic hydrate precipitation model. They calibrate the model to the shift in gas chemistry between Jolliet reservoir gas and gas venting from structures that connect the reservoirs to the Bush Hill vent site. They use the model to predict the profile of subsurface hydrate precipitation and the fraction of gas precipitated. Considering that the hydrate mass accumulated in 10,000 years, they conclude the total venting rate at Jolliet over the last ~10,000 years has been between 900 and 2000 tonnes per year. For a draw of 13.6 km, the total Jolliet venting rate estimated by the analysis presented in Figure 30 is 49 t/a.

The agreement between the two estimates of venting rate is better than it might at first appear. Figure 33 indicates that the calculated venting rate would be doubled (to 100 t/a) if the Jolliet system were sourced by a minibasin with rapid recent sediment deposition,

as is almost certainly the case. It would be increased by a second factor of ~2 (to 210 t/a) if the Jolliet draw were 20 km rather than 13.6 km. If the Bush Hill hydrate mound accumulated in 40,000 years rather than 10,000 years Chen and Cathles minimum system venting rate would be 222 t/a. The two completely independent estimates of total venting rate at Jolliet are thus compatible within reasonable geological uncertainties.

Geological uncertainties have in fact been the bane of all previous attempts to rigorously model petroleum systems. Model interpretations must always be subject to uncertainties that cannot be fully resolved. For example the amounts of kerogen in the Jurassic source beds could be locally higher or lower than estimated. Kerogen chemistry could vary in a fashion that would significantly affect maturation kinetics. The depth of the source beds can be different from that estimated (certainly this is so in cases such as here where primary seismic data constraining the depth are not available). Some geological parameters, such as the pattern of sedimentation, can be constrained, but others will be uncertain. In this context, it is important to appreciate that two-source displacement/mixing models avoid many of these uncertainties. The source richness may be uncertain, but the fraction of expelled hydrocarbons that is retained in migration pathways is independent of this uncertainty. For our models to displace Jurassic oils with Eocene oils, and wash the Eocene oils as observed in the northern half of the GRI corridor, the ratio of the hydrocarbons retained in the migration pathways to those expelled from the source rocks must be less than $\sim 15 \text{ Bt}/131 \text{ Bt} = 0.1$ (see Table 9). The hydrocarbons retained in migration pathways must be a small fraction of those expelled from the source beds. The conclusions that huge quantities of hydrocarbon have vented into the ocean, and that venting hydrocarbons are direct messengers of recent subsurface processes, are robust despite many geological uncertainties.

3. Future Work

The inherent robustness of basin models that simulate the mixing of hydrocarbons from multiple kerogen sources suggests it should be possible to develop a generation of basin models that will be more useful in the exploration process. Our vision for this project was to develop 3D models of each of the study sites, and model the generation and mixing of hydrocarbons, including phase separation, in the sands and faults of these sites in a realistic fashion. The site geological summaries presented in Volume II of this series were made to provide a foundation for these models. Unfortunately work did not progress as rapidly as we had hoped, and the 3D modeling was not accomplished in the timeframe of the current grant.

The vision remains an exciting one, however. Modeling the flow and mixing of both aqueous and hydrocarbon fluids from source, through reservoir, to venting through the sands and faults at a particular site, and predicting the chemistry of hydrocarbons and brines and the rock alteration (see Volume VI of this series) could provide strong constraints on how local systems operate and insights useful in hydrocarbon exploration. For example, the brine salinities are dramatically different in each of the ~15 sands that host oil and gas reservoirs at Eugene Island Block 330. Determining the model conditions that simultaneously replicate the observed brine and hydrocarbon chemistry,

gas washing, and sediment alteration could teach us a lot about how hydrocarbons migrate and vent and provide constraints on the petroleum system that could assist exploration in new, chemically-oriented ways.

Acknowledgements

We thank Exxon for contributing the Louisiana Line section and related data, and ChevronTexaco, particularly Ed Colling, for many discussions related to the modeling. We also thank the member companies of the Global Basins Research Network for their support. Finally we thank Richard Parker of GRI for his advice and support over many years.

References Cited

- Baker, A. J. and D. W. Pepper, 1991, *Finite Elements 1-2-3*: New York, McGraw Hill, 341 pp.
- Bascle, B., L. D. Nixon, et al., 2001, *Atlas of Gulf of Mexico Gas and Oil Sands*, U. S. Department of Interior, Minerals Management Service.
- Blackwell, D. D. and J. L. Steele, 1989, Thermal conductivity of sedimentary rocks: measurement and significance: in N. D. Naeser and T. H. McCulloh, eds., *Thermal History of Sedimentary Basins*: New York, Springer-Verlag, p. 13-36.
- Blatt, H., 1992, *Sedimentary Petrology*: New York, W. H. Freeman, 514 pp.
- Braun, R. L. and A. K. Burnham, 1990, Mathematical model of oil generation, degradation, and expulsion: *Energy and Fuels*, v. 4, p. 132-146.
- Burnham, A. K. and R. L. Braun, 1990, Development of a detailed model of petroleum formation, destruction, and expulsion from lacustrine and marine source rocks: *Organic Geochemistry*, v. 16(1-3), p. 27-39.
- Carslaw, H. S. and J. C. Jaeger, 1959, *Conduction of Heat in Solids*: Oxford, Clarendon Press, 510 pp.
- Cathles, L. M., 1975, *The Viscosity of the Earth's Mantle*: Princeton, Princeton University Press, 386 pp.
- Cathles, L. M., 2001, Capillary seals as a cause of pressure compartmentation in sedimentary basins: *Petroleum Systems of Deep-Water Basins: Global and Gulf of Mexico Experience*, Houston, Texas, GCSSEPM, p. 561-571.
- Coehlo, D. F., 1997, Three dimensional analysis of the temperature field in Block 330, South Eugene Island, Gulf of Mexico: Geological Sciences Ph.D. Thesis, Cornell University, Ithaca, NY, 292 pp.
- Colling, E. L., R. J. Alexander, et al., 2001, Regional Mapping and Maturity Modeling for the Northern Deep Water Gulf of Mexico: *Petroleum Systems of Deep-Water Basins: Global and Gulf of Mexico Experience*, Houston, Texas, GCSSEPM, p. 87-111.
- Cornelius, R. R., L. M. Cathles, et al., accepted, An automated method for inferring 3D salt movements from the supra-salt sedimentation pattern: *AAPG Multidimensional Basin Modeling Proceedings*.
- Deming, D., 1994, Estimation of the thermal conductivity anisotropy of rock with application to the determination of terrestrial heat flow: *Journal of Geophysical Research*, v. 99(B10), p. 22087-22091.
- Demongodin, L., B. Pinoteau, et al., 1991, Thermal conductivity and well logs: A case study in the Paris basin: *Geophysical Journal International*, v. 105, p. 675-691.
- Erendi, A. and L. M. Cathles, 2001, Gas capillary inhibition to oil production: *Petroleum Systems of Deep-Water Basins: Global and Gulf of Mexico Experience*, Houston, Texas, GCSSEPM, p. 607-618.
- Galloway, W., P. Ganey-Curry, et al., 2000, Cenozoic depositional history of the Gulf of Mexico Basin: *AAPG Bulletin*, v. 84, p. 1743-1774.
- Gross, O., K. Hook, et al., 1995, Seismic imaging and analysis of source and migration within an integrated hydrocarbon system study: northern Gulf of Mexico Basin: First Latin American Geophysical Conference, Rio de Janeiro, p. 4.

- Horai, K., 1971, Thermal conductivity of rock-forming minerals: *Journal of Geophysical Research*, v. 76(5), p. 1278-1293.
- Hutchison, I., 1985, The effects of sedimentation and compaction on oceanic heat flow: *Geophysical Journal of the Royal Astronomical Society*, v. 82, p. 439-459.
- Keen, C. E. and T. Lewis, 1982, Measured radiogenic heat production in sediments from continental margin of eastern North America: Implications for petroleum generation: *AAPG Bulletin*, v. 66(9), p. 1402-1407.
- Luo, M., J. R. Wood, et al., 1994, Prediction of thermal conductivity in reservoir rocks using fabric theory: *Journal of Applied Geophysics*, v. 32, p. 321-334.
- McKenna, T. E. and J. M. Sharp, 1998, Radiogenic heat production in sedimentary rocks of the Gulf of Mexico basin: *AAPG Bulletin*, v. 82(3), p. 484-496.
- McKenzie, D., 1978, Some remarks on the development of sedimentary basins: *Earth and Planetary Science Letters*, v. 40, p. 25-32.
- Meulbroek, P., 1997, Hydrocarbon phase fractionation in sedimentary basins: Geological Sciences Ph.D. Thesis, Cornell University, Ithaca, Cornell, 345 pp.
- Meulbroek, P., 1998, Phase fractionation at South Eugene Island Block 330: *Organic Geochemistry*, v. 29, p. 223-229.
- Midttomme, K. and E. Roaldset, 1999, Thermal conductivity of sedimentary rocks: uncertainties in measuring and modeling: in A. C. Aplin, A. J. Fleet and J. H. S. MacQuaker, eds., *Muds and Mudstones: Physical and Fluid Flow Properties*: London, Geological Society London, v. 158, p. 45-60.
- Palciauskas, V. V. and P. A. Domenico, 1989, Fluid pressure in deforming porous rocks: *Water Resources Research*, v. 25(2), p. 203-213.
- Pollack, H. N. and D. S. Chapman, 1977, On the regional variations of heat flow, geotherms, and lithosphere thickness: *Tectonophysics*, v. 38, p. 279-296.
- Revil, A., 2000, Thermal conductivity of unconsolidated sediments with geophysical applications: *Journal of Geophysical Research*, v. 105(B7), p. 16749-16768.
- Revil, A. and L. M. Cathles, 2001, The porosity-depth pattern defined by 40 wells in Eugene Island Aouth Addition, Block 330 Area, and its relation to pore pressure, fluid leakage, and seal migration: *Petroleum Systems of Deep-Water Basins: Global and Gulf of Mexico Experience*, Houston, Texas, GCSSEPM, p. 687-712.
- Royden, L., J. G. Sclater, et al., 1980, Continental margin subsidence and heat flow: important parameters in formation of petroleum hydrocarbons: *AAPG Bulletin*, v. 64(2), p. 173-187.
- Rybach, L., 1976, Radioactive heat production: A physical property determined by the chemistry of rocks: in R. G. J. Strens, ed., *The Physics and Chemistry of Minerals and Rocks*: New York, John Wiley and Sons, p. 309-318.
- Sass, J. H., C. A. Brott, et al., 1981, Heat flow from the crust of the United States: in Y. S. Touloukian, W. R. Judd and R. F. Roy, eds., *Physical Properties of Rocks and Minerals*: New York, McGraw Hill, v. II-2, p. 503-548.
- Shosa, J. D. and L. M. Cathles, 2001, Experimental investigation of capillary blockage of two phase flow in layered porous media: *Petroleum Systems of Deep-Water Basins: Global and Gulf of Mexico Experience*, Houston, Texas, GCSSEPM, p. 721-740.
- Smith, D. L. and W. T. Dees, 1982, Heat flow in the gulf coastal plain: *Journal of Geophysical Research*, v. 87(B9), p. 7687-7693.

- Watts, A. B., 1981, The U.S. Atlantic continental margin: subsidence history, crustal structure and thermal evolution, Atlantic City, AAPG Short Course.
- Winker, C. D., 1982, Cenozoic shelf margins, northwestern Gulf of Mexico: *Gulf Coast Assoc. Geol. Soc. Trans.*, v. 32, p. 427-448.
- Wollenberg, H. A. and A. R. Smith, 1987, Radiogenic heat production: *Geophysical Research Letters*, v. 14(3), p. 295-298.
- Yalcin, M. N., R. Littke, et al., 1997, Thermal history of sedimentary basins: in D. H. Horsfeld, D. R. Baker and D. Welte, eds., *Petroleum and Basin Evolution*: New York, Springer Verlag, p. 73-167.